NASA TECHNICAL NOTE

NASA TN D-3109

NASA TN D-3109

A FREQUENCY INDEPENDENT TECHNIQUE FOR EXTRACTING THE RIGID-BODY MOTION FROM THE TOTAL MOTION OF A LARGE FLEXIBLE LAUNCH VEHICLE

by James C. Howard

Ames Research Center
Moffett Field, Calif.

NATIONAL AERONAUTICS AND SPACE ADMINISTRATION • WASHINGTON, D. C. • NOVEMBER 1965

NASA TN D-3109

A FREQUENCY INDEPENDENT TECHNIQUE FOR EXTRACTING THE RIGID-BODY MOTION FROM THE TOTAL MOTION OF A LARGE FLEXIBLE LAUNCH VEHICLE

By James C. Howard

Ames Research Center
Moffett Field, Calif.

NATIONAL AERONAUTICS AND SPACE ADMINISTRATION

For sale by the Clearinghouse for Federal Scientific and Technical Information
Springfield, Virginia 22151 – Price $3.00

A FREQUENCY INDEPENDENT TECHNIQUE FOR EXTRACTING THE RIGID-BODY MOTION FROM THE TOTAL MOTION OF A LARGE FLEXIBLE LAUNCH VEHICLE

By James C. Howard
Ames Research Center

SUMMARY

A method has been devised for extracting rigid-body motion from combined rigid-body and flexible-body motion. The method involves the use of processing functions and requires that the number of sensing elements be equal to the number of modes of motion considered. Rejection of spurious flexible-body motion is accomplished by making the processing function associated with each sensing element a prescribed function of the modal slopes or the modal displacements. When the processing functions are allocated as prescribed, the information reaching an operator's display panel, or the summing junction where error signals are generated, will not be contaminated by flexible-body motion.

In the first part of the study, it is assumed that the modal data are accurately known. However, uncertainties in the distribution of mass, flexural stiffness, and shear stiffness may give rise to errors in the calculated modal data. Additional errors may result from inaccuracies in the mathematical model used to compute the modal data. An investigation of the influence of modal errors on displays of an example launch vehicle led to the following conclusion. When the rigid-body pitch attitude is equal to, or greater than, the amplitude of the bending motion at the nose of the vehicle, the error in the pitch-attitude display never exceeds 16 percent provided the modal errors do not exceed either +50 percent or -50 percent.

The effect of modal errors on the stability of the controlled system is such that certain combinations of errors tend to degrade the stability of at least one of the bending modes; whereas, other combinations of modal errors tend to enhance stability. The system used for stability analysis included the rigid-body mode and two bending modes. For modal errors of 10 percent or less, and those combinations of modal errors that tend to degrade stability, no instability occurred in either mode when the loop was closed with nominal gain. The results indicate, however, that the first bending mode is more sensitive to errors in the modal data than are the second and, presumably, higher bending modes. These conclusions are based on the assumption that the nominal modal data are used without modification. Examination of the data reveals that it is always possible to insure bending mode stability by a suitable modification of the processing functions to account for an estimated magnitude of modal error. This is equivalent to the use of structural feedback to stabilize the bending modes in the presence of errors in the modal data.

INTRODUCTION

The task of manually controlling a large flexible booster is complicated by the manner in which structural feedback contaminates displays of vehicle motion. Likewise, the control of fully automatic launch vehicles is rendered more difficult by the presence of spurious bending signals at the summing junction where error signals are generated. To eliminate or mitigate flexibility effects, it is necessary to devise a method of extracting rigid-body motion or bending motion from the total motion of a flexible body. Conventionally, this problem has been solved by the use of filters to exclude or attenuate all signals at bending mode frequencies. However, the advent of more flexible launch vehicle configurations has led to a reduction in the gap between the frequencies of the closed-loop rigid-body mode and the frequencies of the elastic modes. Reduction of this gap severely limits the use of conventional filters and requires the invention and development of new techniques for control. Research on this problem at Ames Research Center has been stimulated by the necessity of providing a human operator with displays of rigid-body motion which are not contaminated by spurious bending information.

The primary objectives of the present study are: (1) to describe a frequency independent method for extracting the rigid-body motion from the total motion of a large flexible launch vehicle, (2) to determine the effects of errors in the modal data on displays of rigid-body attitude and attitude rate, and (3) to assess the effect of modal errors on closed-loop system stability.

Other approaches to this problem are described in references 1, 2, and 3.

SYMBOLS

a_j	error coefficient
D_R	rigid-body transfer function
D_1	first bending mode transfer function
D_2	second bending mode transfer function
e	error signal
E	Young's modulus of elasticity
F_j	generalized force
F(s)	filter transfer function
G_A	attitude sensor transfer function
$G_i(s)$	ith attitude sensor transfer function

$G_R(s)$	rate sensor transfer function
$I(x)$	second moment of area
j	$\sqrt{-1}$
K_j	generalized stiffness
K_{p1}	pitching-moment coefficient
K_{q_p}	attitude gain
$K_{\dot{q}_p}$	attitude rate gain
K_R	ratio of attitude rate gain to attitude gain
K_{11}	generalized force coefficient for the first bending mode
K_{12}	engine inertia coefficient for the first bending mode
K_{21}	generalized force coefficient for the second bending mode
K_{22}	engine inertia coefficient for the second bending mode
$m(x)$	mass per unit length
M_j	generalized mass
$P(x,t)$	lateral force distribution
$P_{pi}(\psi)$	function for processing the output of attitude and attitude-rate sensors
$P_{pi}(\varphi)$	function for processing accelerometer outputs in order to obtain rigid-body pitching acceleration
$P_{Ti}(\varphi)$	function for processing accelerometer outputs in order to obtain rigid-body translational acceleration
$\Delta P_{pi}(\psi)$	increment in $P_{pi}(\psi)$
q_j	generalized coordinate
δq_p	increment in the pitch attitude
δq_{pj}	pitch-attitude display error due to errors in jth modal slope
$[Q]$	column vector consisting of the rigid-body pitch attitude and the n generalized coordinates
s	complex frequency, $\sigma + j\omega$

$S(s)$	servo transfer function
t	time
x	distance measured along the longitudinal axis
x_{cg}	center-of-gravity location
$y(x,t)$	bending deflection at section x and at time t
δ	thrust vector deflection
Δ	determinant
ζ_R	rate sensor damping
ζ_j	structural damping ratio
θ_{Bi}	bending angle at sensor location i
θ_{BN}	bending angle at the nose
θ_c	commanded pitch attitude
θ_F	feedback signal
θ_i	output of an attitude sensor
θ_{Nj}	bending angle at nose in jth mode
$[\Theta]$	column vector of measured angular displacements
σ	real component of frequency vector
φ_{ij}	value of the jth modal displacement function at location x_i
$\varphi_j(x)$	jth modal displacement function
Φ_{ij}	cofactor corresponding to φ_{ij}
$[\psi]$	matrix operator, the elements of which are the modal slopes at the sensor locations
ψ_{ij}	value of the jth modal slope function at location x_i
$\psi_j(x)$	jth modal slope function
Ψ_{ij}	cofactor corresponding to ψ_{ij}
ω	imaginary component of frequency vector
ω_f	break frequency of first-order filter

ω_j natural frequency of jth structural mode

ω_R rate sensor frequency

ω_s break frequency of first-order servo

Subscripts

A accelerated motion

B magnitude of the subscripted variable resulting from bending

cg center of gravity

C commanded value of the subscripted variable

i location at which subscripted function is evaluated

j denotes which bending mode the subscripted modal function describes

n general term of a series of modal functions

N magnitude of the subscripted variable at the nose

P pitching motion

R rate information

T translation

Superscript

$(\dot{})$ derivative with respect to time

METHOD

The method proposed in the present report for extracting rigid-body motion from the total motion of a flexible body uses the series expansion of the motion of the elastic system in terms of the normal modes and the generalized coordinates. In the present context, a normal mode of free vibration is the spatial function or shape a vibrating beam assumes when it is oscillating at one of its natural frequencies. The generalized coordinates are the time functions or the functions that describe the variation of modal amplitude with time. The normal modes of free vibration of an elastic system can be computed when the distribution of mass, flexural stiffness, and shear stiffness are known. Hence, the modal functions can be obtained for any elastic system being considered. By equating measured sensor outputs to the motion described in terms of a series of normal modes and generalized coordinates, a system

of equations is obtained which can be solved for the rigid-body components of the motion, if the number of sensors equals the number of terms of the series. It is not anticipated, however, that more than a few terms of the series will be necessary, since high frequency bending signals can be eliminated, if necessary, by conventional filtering techniques. The solution of this system of equations is presented in the form of a series of products of processing functions and sensor outputs. The processing functions operate on the sensor outputs in such a way that the sum of the processed outputs gives the rigid-body motion.

The advantages of the proposed method are its simplicity and the absence of any need for on-board computational capability. All that is required is that the processing function associated with each sensor be a prescribed function of the modal data at the sensor location. Since the modal data is a known function of position along the length of the vehicle structure, the processing functions may be precomputed, and hence no auxiliary on-board computing equipment is required. By the use of this method, separation and rejection of bending motion is accomplished even in situations where a bending frequency coincides with the frequency of the closed-loop rigid-body mode. It is not necessary to know the frequencies of the elastic modes since the method does not rely on the relative frequencies of the closed-loop rigid-body control mode and the elastic modes. Instead, the method uses the known modal properties of the structure being controlled, and consequently is well adapted to situations where a body bending frequency coincides with or differs only slightly from the control mode frequency.

ANALYSIS

Equations of Motion

When a beam is vibrating under the influence of a concentrated or a distributed forcing function, the total displacement can be described in terms of the normal modes of free vibration and the generalized coordinates. A normal mode of vibration is the space function or shape the vibrating beam assumes when it is oscillating at one of its natural frequencies. In figure 1 are shown the first three bending modes of a uniform free-free beam. The generalized coordinates are the functions which describe the variation of modal amplitude with time. These functions can be obtained by solving the partial differential equation of motion for an elastic beam which is moving under the influence of concentrated or distributed forcing functions. If shear deformation and rotary inertia are neglected, the plane elastic motion of a continuous beam is described by the following partial differential equation, see reference 4.

$$\frac{\partial^2}{\partial x^2} EI(x) \frac{\partial^2 y(x,t)}{\partial x^2} + m(x) \frac{\partial^2 y(x,t)}{\partial t^2} = P(x,t) \qquad (1)$$

The normal modes of vibration are obtained by solving the partial differential equation of motion for the free oscillations of an elastic beam. The relevant equation is

$$\frac{\partial^2}{\partial x^2} EI(x) \frac{\partial^2 y(x,t)}{\partial x^2} + m(x) \frac{\partial^2 y(x,t)}{\partial t^2} = 0 \tag{2}$$

A solution to this equation may be obtained by assuming that the variables are separable and by using the appropriate boundary conditions for the beam. A free-free beam is characterized by the absence of end constraints, that is, the bending moments and shear forces are zero at each end. With the use of these boundary conditions, equation (2) may be solved to obtain the spatial functions which may then be used to describe the displacement of a beam which is undergoing forced oscillations. In terms of the displacement and time functions, the total bending displacement is given by

$$y(x,t) = \sum_{j=1}^{\infty} \varphi_j(x) q_j(t) \tag{3}$$

where $\varphi_j(x)$ are the modal displacement functions and $q_j(t)$ are the generalized coordinates, or the functions which describe the variation of modal amplitude with time.

Differential Equation for the Generalized Coordinates

Upon substitution from equation (3) in equation (1), the following equation is obtained

$$\frac{\partial^2}{\partial x^2} EI(x) \frac{\partial^2}{\partial x^2} \sum_{j=1}^{\infty} \varphi_j(x) q_j(t) + m(x) \frac{\partial^2}{\partial t^2} \sum_{j=1}^{\infty} \varphi_j(x) q_j(t) = P(x,t) \tag{4}$$

When each side of equation (4) is multiplied by $\varphi_i(x)$ and integrated over the length of the beam, taking advantage of the orthogonal property of the normal modes, the equation of motion for the jth mode assumes the following form

$$M_j \ddot{q}_j(t) + K_j q_j(t) = F_j(t) \tag{5}$$

where M_j is the generalized mass of the beam in the jth mode of vibration. A dot denotes differentiation with respect to time. The generalized stiffness and the generalized forcing function in the jth mode of vibration are K_j and F_j, respectively. These quantities are defined as follows

$$M_j = \int m(x)\varphi_j^2(x)dx \tag{6}$$

$$K_j = \int \varphi_j(x)\left[\frac{\partial^2}{\partial x^2} EI(x) \frac{\partial^2 \varphi_j(x)}{\partial x^2}\right]dx \tag{7}$$

$$F_j(t) = \int P(x,t)\varphi_j(x)dx \tag{8}$$

where the integrals are taken over the length of the beam. Equation (6) does not include the effects of rotary inertia, nor does equation (7) reflect the influence of shear deformation. Although shear deformation and rotary inertia should, in general, be included in any mathematical model which is being used to determine modal data, a discussion of these effects is not relevant to the present investigation, where the main objective is to process measured sensor outputs in such a way that rigid-body motion is extracted from combined rigid-body and bending motion. The preceding simplified presentation is used only to elucidate the arguments which follow. For a complete derivation of the equations of motion of an elastic beam, the reader is referred to references 4 through 8. Equation (5) may be rewritten as follows

$$\ddot{q}_j(t) + \omega_j^2 q_j(t) = \frac{F_j(t)}{M_j} \tag{9}$$

$$\omega_j^2 = \frac{K_j}{M_j} \tag{10}$$

where ω_j is the natural frequency of the jth free-free mode. The external forcing function consists of all aerodynamic forces, thrust forces, engine control-servo inertia forces, and propellant sloshing forces.

Structural damping.- In practice, an elastic beam will possess some dissipative forces which provide damping. Since the dissipative energy is usually small in comparison to the elastic and kinetic energies, the lower modes will be very lightly damped. The dissipative force can be taken into account by adding a small viscous damping term to equation (9). When this is done equation (9) assumes the following form

$$\ddot{q}_j + 2\zeta_j\omega_j\dot{q}_j + \omega_j^2 q_j = \frac{F_j}{M_j} \tag{11}$$

where ζ_j is the damping ratio in the jth bending mode. A value of $\zeta_j = 0.005$ was assumed in the present study.

Total displacement of an elastic beam which describes forced oscillations.- In terms of the normal modes and the corresponding generalized coordinates, the total displacement can be expressed as follows

$$y(x,t) = \sum_{j=T,P,1}^{n} \varphi_j(x) q_j(t) \tag{12}$$

where the normal modes are understood to include the rigid-body mode of translation of the center of gravity, and the rigid-body mode of rotation of the beam about its center of gravity. In this formulation, the normal mode of translation is unity and the corresponding generalized coordinate is q_T. In the rotational mode, the normal mode is $x - x_{cg}$ and the corresponding generalized coordinate is q_p. Equation (9) can still be used to describe the rigid-body modes, provided

$$\omega_T = \omega_P = 0 \tag{13}$$

where ω_T is the frequency of the translational mode and ω_P is the frequency of the pitching mode. Note that all the aerodynamic forces are included in the external forcing function $F_j(t)$. In view of these comments, equation (12) can be expanded as follows

$$y(x,t) = q_T + (x - x_{cg}) q_p + \sum_{j=1}^{n} \varphi_j(x) q_j(t) \tag{14}$$

Separation of Rigid-Body and Bending Motion

Angular displacements.- Let it be assumed that equation (2) has been solved and that modal displacement functions and modal slope functions are available. If θ_i denotes the measured output from an attitude sensor located at station i on the structure, then on differentiating equation (14) with respect to x, the total angular displacement at location i is obtained in the following form

$$\theta_i = \frac{\partial y}{\partial x} = q_p + \frac{\partial \varphi_1(x_i)}{\partial x} q_1 + \cdots + \frac{\partial \varphi_n(x_i)}{\partial x} q_n \tag{15}$$

that is

$$\theta_i = q_p + \sum_{j=1}^{n} \frac{\partial \varphi_j(x_i)}{\partial x} q_j(t) \tag{16}$$

If $\partial \varphi_j(x_i)/\partial x$ is denoted by ψ_{ij}, where $\psi_{ij} = \psi_j(x_i)$ is the modal slope for the jth bending mode at location i, equation (16) may be rewritten as follows

$$\theta_i = q_p + \sum_{j=1}^{n} \psi_{ij}(x) q_j(t) \tag{17}$$

The measured output θ_i is seen to consist of (n+1) unknown components, that is, there is the unknown pitching angle q_p and the n generalized coordinates q_j. However, a solution to equation (17) is possible if (n+1) sensors are used at (n+1) distinct locations. In this case there would be (n+1) measured outputs θ_i, giving rise to (n+1) equations for the (n+1) unknowns as follows

$$\begin{pmatrix} \theta_1 \\ \theta_2 \\ \theta_3 \\ \cdot \\ \cdot \\ \cdot \\ \theta_n \\ \theta_{n+1} \end{pmatrix} = \begin{pmatrix} 1 & \psi_{11} & \psi_{12} & \cdots & \psi_{1n} \\ 1 & \psi_{21} & \psi_{22} & \cdots & \psi_{2n} \\ 1 & \psi_{31} & \psi_{32} & \cdots & \psi_{3n} \\ \cdot & \cdot & \cdot & \cdots & \cdot \\ \cdot & \cdot & \cdot & \cdots & \cdot \\ \cdot & \cdot & \cdot & \cdots & \cdot \\ 1 & \psi_{n1} & \psi_{n2} & \cdots & \psi_{nn} \\ 1 & \psi_{n+1,1} & \psi_{n+1,2} & \cdots & \psi_{n+1,n} \end{pmatrix} \begin{pmatrix} q_p \\ q_1 \\ q_2 \\ \cdot \\ \cdot \\ \cdot \\ \cdot \\ q_n \end{pmatrix} \tag{18}$$

This matrix equation can be solved to determine the unknown rigid-body rotation and the n generalized coordinates as functions of the measured outputs from the sensors and the known modal data. Equation (18) may be written in abbreviated form as follows

$$[\Theta] = [\psi][Q] \tag{19}$$

where $[\Theta]$ is a column vector of measured angular displacements, and $[Q]$ is a column vector consisting of the rigid-body pitch attitude and the n generalized coordinates. To simplify the formulation, the first column of the matrix operator $[\psi]$ may be redefined to give

$$[\psi] = \begin{pmatrix} \psi_{10} & \psi_{11} & \psi_{12} & \cdots & \psi_{1n} \\ \psi_{20} & \psi_{21} & \psi_{22} & \cdots & \psi_{2n} \\ \psi_{30} & \psi_{31} & \psi_{32} & \cdots & \psi_{3n} \\ \cdot & \cdot & \cdot & \cdots & \cdot \\ \cdot & \cdot & \cdot & \cdots & \cdot \\ \cdot & \cdot & \cdot & \cdots & \cdot \\ \psi_{no} & \psi_{n1} & \psi_{n2} & \cdots & \psi_{nn} \\ \psi_{n+1,o} & \psi_{n+1,1} & \psi_{n+1,2} & \cdots & \psi_{n+1,n} \end{pmatrix} \tag{20}$$

where $\psi_{jo} = 1$ for $j=1, 2, \ldots, n+1$. From equation (19), the column vector $[Q]$ is obtained in the following form

$$[Q] = [\psi]^{-1}[\Theta] \tag{21}$$

The inverse of the matrix $[\psi]$ is given by

$$[\psi]^{-1} = \frac{1}{\Delta_p} \begin{pmatrix} \Psi_{10} & \Psi_{20} & \Psi_{30} & \vdots\ \vdots\ \vdots & \Psi_{no} & \Psi_{n+1,o} \\ \Psi_{11} & \Psi_{21} & \Psi_{31} & \cdot\ \vdots\ \vdots & \Psi_{n1} & \Psi_{n+1,1} \\ \Psi_{12} & \Psi_{22} & \Psi_{32} & \vdots\ \vdots\ \vdots & \Psi_{n2} & \Psi_{n+1,2} \\ \cdot & \cdot & \cdot & \cdots & \cdot & \cdot \\ \cdot & \cdot & \cdot & \cdots & \cdot & \cdot \\ \cdot & \cdot & \cdot & \cdots & \cdot & \cdot \\ \Psi_{1n} & \Psi_{2n} & \Psi_{3n} & \cdots & \Psi_{nn} & \Psi_{n+1,n} \end{pmatrix} \tag{22}$$

where Ψ_{ij} is the cofactor of the element ψ_{ij} in the matrix $[\psi]$, and Δ_p is the determinant of $[\psi]$. Upon substitution from equation (22) in equation (21), the rigid-body rotation is obtained in the form of a series as follows

$$q_p = \frac{1}{\Delta_p}\left(\Psi_{1o}\theta_1 + \Psi_{2o}\theta_2 + \cdots \Psi_{n+1,o}\theta_{n+1}\right)$$

that is,

$$q_p = \frac{1}{\Delta_p}\sum_{i=1}^{n+1}\Psi_{io}\theta_i \tag{23}$$

The coefficient of θ_i in equation (23) will be denoted by $P_{pi}(\psi)$, and will subsequently be referred to as an attitude processing function, since this function is used to process the output from an attitude sensor located at x_i. With this notation, equation (23) may be rewritten as follows

$$q_p = \sum_{i=1}^{n+1} P_{pi}(\psi)\theta_i \tag{24}$$

where

$$P_{pi}(\psi) = \frac{\Psi_{io}}{\Delta_p} \tag{25}$$

Special case.- To illustrate the method, equation (18) will be solved for the case where $i=3$ and $j=2$. This is tantamount to the assumption that bending modes higher than the second may be neglected. With these values of the subscripts, equation (18) reduces to

$$\begin{pmatrix}\theta_1\\ \theta_2\\ \theta_3\end{pmatrix} = \begin{pmatrix}1 & \psi_{11} & \psi_{12}\\ 1 & \psi_{21} & \psi_{22}\\ 1 & \psi_{31} & \psi_{32}\end{pmatrix}\begin{pmatrix}q_p\\ q_1\\ q_2\end{pmatrix} = \begin{pmatrix}\Psi_{1o} & \Psi_{11} & \Psi_{12}\\ \Psi_{2o} & \Psi_{21} & \Psi_{22}\\ \Psi_{3o} & \Psi_{31} & \Psi_{32}\end{pmatrix}\begin{pmatrix}q_p\\ q_1\\ q_2\end{pmatrix} \tag{26}$$

therefore,

$$\begin{pmatrix}q_p\\ q_1\\ q_2\end{pmatrix} = \frac{1}{\Delta_p}\begin{pmatrix}\Psi_{1o} & \Psi_{2o} & \Psi_{3o}\\ \Psi_{11} & \Psi_{21} & \Psi_{31}\\ \Psi_{12} & \Psi_{22} & \Psi_{32}\end{pmatrix}\begin{pmatrix}\theta_1\\ \theta_2\\ \theta_3\end{pmatrix} \tag{27}$$

In this case, equation (24) consists of three terms. Hence,

$$q_p = \sum_{i=1}^{3} P_{pi}(\psi)\theta_i \tag{28}$$

where

$$P_{p1}(\psi) = \frac{\Psi_{10}}{\Delta_p} = \frac{(\psi_{21}\psi_{32} - \psi_{22}\psi_{31})}{\Delta_p} \tag{29}$$

$$P_{p2}(\psi) = \frac{\Psi_{20}}{\Delta_p} = \frac{-(\psi_{11}\psi_{32} - \psi_{12}\psi_{31})}{\Delta_p} \tag{30}$$

$$P_{p3}(\psi) = \frac{\Psi_{30}}{\Delta_p} = \frac{(\psi_{11}\psi_{22} - \psi_{12}\psi_{21})}{\Delta_p} \tag{31}$$

and

$$\Delta_p = [(\psi_{21}\psi_{32} - \psi_{22}\psi_{31}) - (\psi_{11}\psi_{32} - \psi_{12}\psi_{31}) + (\psi_{11}\psi_{22} - \psi_{12}\psi_{21})] \tag{32}$$

These are the attitude processing functions or gains to be used with the outputs θ_1, θ_2, and θ_3, respectively. When the outputs from the three attitude sensors are processed in the manner described, the information reaching an operator's display panel, or the summing junction where error signals are generated will be rigid-body information only. Of course, this is contingent on the validity of the assumption that the motion of the system can be adequately represented by two bending modes. It can be seen that the attitude processing functions depend only on the modal slopes. Hence, these functions can be computed and stored prior to launch. Variation of modal data during flight may require that the appropriate processing functions be programmed to compensate for these variations. The sensitivity of the processing functions to changes in the modal data will be discussed later.

Angular rates.- If $\dot{\theta}_i$ denotes the output from an angular rate sensor located at x_i on the elastic structure, then differentiation of equation (17) with respect to time yields the equation for the angular rates in the following form

$$\dot{\theta}_i = \dot{q}_p + \sum_{j=1}^{n} \psi_{ij}(x)\dot{q}_j(t) \tag{33}$$

As in the case of angular displacements, the solution of the angular rate problem requires that (n+1) rate sensors be used at (n+1) distinct locations.

The information obtained from this number of sensors is the amount required to permit separation of rigid-body rates from combined rigid-body and bending rates, by providing (n+1) equations for the (n+1) unknowns. The measured angular rates are related to the rigid-body pitching rate and the rates of change of the generalized coordinates in the same manner in which the angular displacements are related to the pitch attitude and the generalized coordinates. Hence,

$$[\dot{\Theta}] = [\psi][\dot{Q}] \tag{34}$$

where $[\dot{\Theta}]$ is a column vector of measured angular rates, and $[\dot{Q}]$ is a column vector consisting of the rigid-body pitching rate and the rates of change of the generalized coordinates. The matrix $[\psi]$ is defined in equation (20) where $\psi_{io} = 1$ for i=1, 2, . . . , n+1. Equation (34) can be solved to obtain the column vector of unknown rates $[\dot{Q}]$ in terms of the measured rates and the known modal slopes

$$[\dot{Q}] = [\psi]^{-1}[\dot{\Theta}] \tag{35}$$

where $[\psi]^{-1}$ is given by equation (22). It follows that the measured angular rates are processed in the same manner as the measured angular displacements. Therefore

$$\dot{q}_p = \sum_{i=1}^{n+1} P_{pi}(\psi)\dot{\theta}_i \tag{36}$$

where the processing functions $P_{pi}(\psi)$ have the values given by equation (25).

The block diagram of figure 2 indicates how the rigid-body pitch rate may be extracted from the total motion of a flexible body. The three rate sensors are assumed to have transfer functions of the form shown. It is seen that the rigid-body pitch rate is obtained by weighting the output of each sensor by the appropriate processing function and summing. The functional forms $P_{pi}(\psi)$ of the processing functions are shown in the figure. The blocks G_i, i=1,2,3, represent the attitude sensors to be used in conjunction with the corresponding processing functions to give rigid-body pitch attitude. In cases where it is desirable to supplement the attitude and attitude-rate information with acceleration feedback, the output of a suitable number of accelerometers must be processed in order to extract the rigid-body acceleration from the total acceleration of a flexible body. The method is similar to that described for obtaining rigid-body attitudes and attitude rates from the outputs of attitude and attitude-rate sensors. However, because of the fact that the rigid-body acceleration consists of a translational and rotational component, an additional sensor is required to provide sufficient information for determining the rigid-body components of acceleration. The method is described in appendix A, where the processing functions required to extract rigid-body acceleration from accelerometer outputs are derived for the general case of the two rigid-body mode components and n bending mode components.

APPLICATION OF RESULTS OF ERROR ANALYSIS TO A LARGE FLEXIBLE BOOSTER

Influence of Errors in the Modal Data on Displays of Vehicle Motion

Since errors in the modal data give rise to errors in the processing functions, and hence to display errors and errors in the feedback control signal, it is necessary to examine the influence of these errors on displays of vehicle motion and on the stability of the closed-loop system. In this section, the influence of errors on displays of vehicle motion will be considered.

The influence of errors in the modal data on displays of vehicle motion was computed for a model vehicle. The model vehicle which is representative of a typical large flexible space vehicle booster, and which was supplied by the Aero-Astrodynamics Laboratory of the Marshall Space Flight Center, is similar to or larger than the Saturn vehicle, but is not intended to represent any specific vehicle. The modal data for this vehicle is shown in table 1 for a flight time of 80 seconds. To produce meaningful results, the locations chosen for the sensors represent possible sensor locations for the model booster configuration (see fig. 3). For the following computations, the sensors were located at distances of 19.3, 48.1, and 69.7 meters from the gimbal axis.

Attitude errors and attitude-rate errors resulting from inaccuracies in the modal data.- An IBM 7090 digital computer was used to compute the attitude processing functions for a system with two bending modes. The initial computations were for nominal values of the modal slopes at three distinct sensor locations. Since the influence of errors in the modal data on computed values of the processing functions depends on which modal slope or group of modal slopes is in error, the computations must be sufficiently comprehensive to include all possible combinations of modal slopes. For three attitude sensors and with the assumption that modal excitation is confined to the first two bending modes, a total of six modal slopes is required to compute the three processing functions. In this case, a total of (2^6-1) combinations of modal slopes is possible. Hence, if the percent error assigned to each member of a group of modal slopes can assume a positive or a negative value, it would be necessary to compute each processing function 63 times for each percentage error assumed in the corresponding members of the group. However, if it is assumed that the percent error in each member of a group of modal slopes has the same sign, relationships between the errors in different groups of modal slopes can be established. Because of these relationships, the number of computations can be reduced as follows: If ψ_{ij} is assumed to have an error of n percent subject to the constraint that all other modal slopes are free from error, an error in the remaining slopes from the same mode can be related to the assumed error in ψ_{ij}. The slope at sensor location 1 in mode j is denoted by ψ_{1j}. Subsequent to the introduction of an n percent error, the slope at ψ_{1j} becomes $(1+n/100)\,\psi_{1j}$. If the jth modal slope function is now normalized to ψ_{1j} at sensor location 1, the slopes at sensor locations 2 and 3, in mode j, assume the values $\psi_{2j}/(1+n/100)$ and $\psi_{3j}/(1+n/100)$,

respectively. Hence, an error of n percent in ψ_{1j} is equivalent to an error of N percent in the slopes ψ_{2j} and ψ_{3j}, where

$$N = -\frac{100n}{100 + n} \tag{37}$$

Similar reasoning shows that an n percent error in ψ_{2j} is equivalent to an N percent error in ψ_{1j} and ψ_{3j}. Likewise, an error of n percent in ψ_{3j} is equivalent to an N percent error in ψ_{1j} and ψ_{2j}. Consequently, a given percentage error in a single modal slope has the same influence on the processing functions as an equivalent percentage error in each member of a group of two modal slopes as follows:

$$\psi_{11} \propto \psi_{21}\psi_{31}$$

$$\psi_{12} \propto \psi_{22}\psi_{32}$$

$$\psi_{21} \propto \psi_{11}\psi_{31}$$

$$\psi_{22} \propto \psi_{12}\psi_{32}$$

$$\psi_{31} \propto \psi_{11}\psi_{21}$$

$$\psi_{32} \propto \psi_{12}\psi_{22}$$

Therefore, out of a total of 15 pairs of modal slopes, the errors in 6 of these are related to the errors in the modal slopes taken one at a time. Hence, it is only necessary to consider errors in the remaining 9 pairs of modal slopes. As a consequence of similar reasoning applied to the remaining groups of modal slopes, it can be shown that out of a total of 63 possible combinations of modal slopes, it is only necessary to consider 24 of these. Of course, these computations would apply to only one set of sensor locations. If a range of sensor locations were considered, the computations would have to be repeated for each set of locations.

Errors in the processing functions interpreted as display errors.- By referring to figure 4, it can be seen that the attitude error per degree of attitude sensor output, or the rate error per degree per second of rate sensor output. is simply the error ΔP_i induced in the processing function P_i by errors in the modal data. The combined effect of these errors is given by

$$\delta q_p = \sum_{i=1}^{3} \Delta P_{pi}\theta_i = \sum_{i=1}^{3} \Delta P_{pi}(q_p + \theta_{Bi}) \tag{38}$$

ψ true value of ψ

$\Delta\psi$ assumed error in ψ

ΔP_{pi} $P_{pi}(\psi + \Delta\psi) - P_{pi}(\psi)$

θ_{Bi} is the bending angle at sensor location i, that is

$$\theta_{Bi} = (\psi_{i1}q_1 + \psi_{i2}q_2) = \sum_{j=1}^{2} \psi_{ij}q_j$$

The equation for δq_p may be rewritten as follows

$$\delta q_p = q_p \sum_{i=1}^{3} \Delta P_{pi} + \sum_{i=1}^{3} \theta_{Bi} \Delta P_{pi}$$

It can be shown that $\sum_{i=1}^{3} \Delta P_{pi} = 0$; therefore this equation reduces to the simpler form

$$\delta q_p = \sum_{i=1}^{3} \theta_{Bi} \Delta P_{pi} = \sum_{i=1}^{3} \sum_{j=1}^{2} \psi_{ij}q_j \Delta P_{pi}$$

therefore

$$\delta q_p = \sum_{j=1}^{2} q_j \sum_{i=1}^{3} \psi_{ij} \Delta P_{pi} = \sum_{j=1}^{2} a_j q_j \qquad (39)$$

where

$$a_j = \sum_{i=1}^{3} \psi_{ij} \Delta P_{pi} \qquad (40)$$

This equation may be used to relate δq_p to the bending angle at some reference location. If the nose of the vehicle is chosen as the reference location, and if θ_{BN} denotes the bending angle at this location, then

$$\theta_{BN} = \sum_{j=1}^{2} \psi_{Nj}q_j = \sum_{j=1}^{2} \theta_{Nj}$$

where $\theta_{Nj} = \psi_{Nj}q_j$ is the bending angle at the nose in the jth mode. Equation (39) may be rewritten in the following form

$$\delta q_p = \sum_{j=1}^{2} \frac{a_j}{\psi_{Nj}} (\psi_{Nj} q_j) = \sum_{j=1}^{2} \frac{a_j}{\psi_{Nj}} \theta_{Nj} = \sum_{j=1}^{2} \delta q_{pj} \theta_{Nj} \tag{41}$$

where

$$\delta q_{pj} = \frac{a_j}{\psi_{Nj}} \tag{42}$$

Numerical Results

It is seen that δq_{pj} is a measure of the error in the rigid-body pitch-attitude display per degree of bending at the nose in the jth mode. Likewise, δq_{pj} may be interpreted as the error in the rigid-body pitch-rate display, per degree per second of bending rate at the nose, in the jth mode. If there are no errors in the modal data, these coefficients are zero and the bending motion is completely filtered out. When the data corresponding to a flight time of 80 seconds was processed, the values of the coefficients shown in table 2 were obtained. The computed values of these coefficients are tabulated as a function of the percentage errors in a given modal slope or group of modal slopes. It is seen that when the amplitude of the rigid-body pitch attitude is greater than, or equal to, the bending motion at the nose of the vehicle, the error in the pitch attitude display never exceeds 16 percent if modal slope errors do not exceed either +50 percent or -50 percent.

Influence of Errors in the Modal Data on the Stability of the Closed-Loop System

Analysis.- From figure 4 it is seen that if θ_i denotes the total angular displacement as seen at the ith sensor, then from equation (17)

$$\theta_i = q_p + \sum_{j=1}^{2} \psi_{ij} q_j \tag{43}$$

Therefore,

$$\theta_1 = q_p + \psi_{11} q_1 + \psi_{12} q_2$$

$$\theta_2 = q_p + \psi_{21} q_1 + \psi_{22} q_2$$

$$\theta_3 = q_p + \psi_{31} q_1 + \psi_{32} q_2$$

For the case considered, the air-frame dynamics may be represented by three parallel elements as shown in sketch (a).

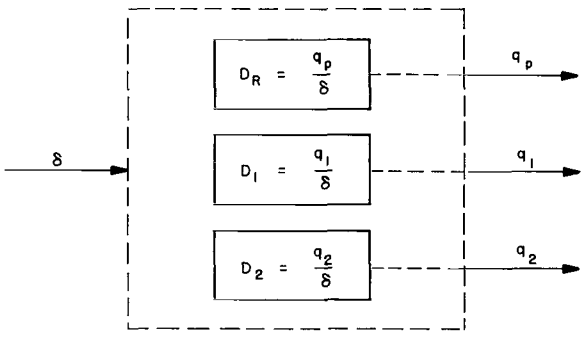

Sketch (a)

D_R rigid-body transfer function

D_1 first bending mode transfer function

D_2 second bending mode transfer function

From equation (43)

$$\frac{\theta_i}{\delta} = \frac{q_p}{\delta} + \sum_{j=1}^{2} \psi_{ij} \frac{q_j}{\delta} \qquad (44)$$

where δ is the thrust vector deflection. Therefore

$$\theta_1/\delta = D_R + \psi_{11}D_1 + \psi_{12}D_2$$

$$\theta_2/\delta = D_R + \psi_{21}D_1 + \psi_{22}D_2$$

$$\theta_3/\delta = D_R + \psi_{31}D_1 + \psi_{32}D_2$$

From figure 4, it is seen that if the rate feedback loop is omitted, the open-loop transfer function is given by

$$\frac{\theta_F}{e} = F(s)S(s)\Big\{G_1(D_R + \psi_{11}D_1 + \psi_{12}D_2)\Big[P_{pi}(\psi) + \Delta P_{pi}(\psi)\Big] + G_2(D_R + \psi_{21}D_1 + \psi_{22}D_2)\Big[P_{pi}(\psi) + \Delta P_{pi}(\psi)\Big] + G_3(D_R + \psi_{31}D_1 + \psi_{32}D_2)\Big[P_{pi}(\psi) + \Delta P_{pi}(\psi)\Big]\Big\}K_{q_p} \qquad (45)$$

i = 1, 2, or 3 in first, second, or third group, respectively.

θ_F feedback signal

e error signal

F(s) filter transfer function

S(s) servo-transfer function

G_i attitude sensor transfer function

K_{q_p} pitch attitude gain

With the assumption that the attitude sensors have the same transfer function, that is, $G_1 = G_2 = G_3 = G_A$, equation (45) can be rewritten as

$$\frac{\theta_F}{e} = F(s)S(s)G_A\left[D_R \sum_{i=1}^{3} P_{pi}(\psi) + D_R \sum_{i=1}^{3} \Delta P_{pi}(\psi) + D_1 \sum_{i=1}^{3} \psi_{i1} P_{pi}(\psi)\right.$$

$$\left. + D_1 \sum_{i=1}^{3} \psi_{i1} \Delta P_{pi}(\psi) + D_2 \sum_{i=1}^{3} \psi_{i2} P_{pi}(\psi) + D_2 \sum_{i=1}^{3} \psi_{i2} \Delta P_{pi}(\psi)\right] Kq_p$$

However, by using equations (29) through (32) and the definition of $\Delta P_{pi}(\psi)$, it can be verified that

$$\sum_{i=1}^{3} \Delta P_{pi}(\psi) = \sum_{i=1}^{3} \psi_{i1} P_{pi}(\psi) = \sum_{i=1}^{3} \psi_{i2} P_{pi}(\psi) = 0 \tag{46}$$

and

$$\sum_{i=1}^{3} P_{pi}(\psi) = 1 \tag{47}$$

(It is interesting to note that $\sum_{i=1}^{3} \Delta P_{pi}(\psi) = 0$. This implies that in the absence of bending, the rigid-body display will not be affected by errors in the processing functions induced by errors in the modal data.) Therefore,

$$\frac{\theta_F}{e} = F(s)S(s)G_A\left[D_R + D_1 \sum_{i=1}^{3} \psi_{i1} \Delta P_{pi}(\psi) + D_2 \sum_{i=1}^{3} \psi_{i2} \Delta P_{pi}(\psi)\right] Kq_p \tag{48}$$

As defined in equation (40)

$$a_1 = \sum_{i=1}^{3} \psi_{i1} \Delta P_{pi}(\psi) \tag{49}$$

$$a_2 = \sum_{i=1}^{3} \psi_{i2} \Delta P_{pi}(\psi) \tag{50}$$

therefore,

$$\frac{\theta_F}{e} = [F(s)S(s)G_A(D_R + a_1D_1 + a_2D_2)]K_{q_p} \tag{51}$$

If attitude rate feedback is included, the open-loop transfer function must be modified accordingly. In this case

$$\frac{\theta_F}{e} = \left[F(s)S(s)\left(D_R + \sum_{j=1}^{2} a_jD_j\right)(G_A + K_Rs G_R)\right]K_{q_p} \tag{52}$$

where

$$K_R = \frac{K_{\dot{q}_p}}{K_{q_p}}$$

and

$$G_R = \frac{\omega_R^2}{s^2 + 2\zeta_R\omega_R s + \omega_R^2} = \frac{1}{\left(\frac{s}{\omega_R}\right)^2 + 2\zeta_R\left(\frac{s}{\omega_R}\right) + 1}$$

Since principal structural and control system frequencies are very much less than ω_R it is permissible to assume for present purposes that $G_R = 1$. Likewise, because of the absence of free gyro dynamics, the attitude transfer function also assumes the form $G_A = 1$. When these substitutions are made in equation (52), the open-loop transfer function assumes the form

$$\frac{\theta_F}{e} = \left[F(s)S(s)\left(D_R + \sum_{j=1}^{2} a_jD_j\right)(1 + K_Rs)\right]K_{q_p} \tag{53}$$

Transfer function formulation.- For the purpose of ascertaining the influence of the error coefficients a_j on the stability of the closed-loop system, an approximate transfer function for the system shown in figure 4 was used. The filter transfer function $F(s)$ and the servo-transfer function $S(s)$ were both assumed to be first-order lags. In formulating the rigid-body transfer function $D_R(s)$, engine inertia and aerodynamic effects were omitted. The first and second bending mode dynamics were treated as second-order systems in which engine inertia and structural damping were included. The open-loop transfer function given by equation (53) consists of the following elements:

$$F(s) = \frac{\omega_f}{s + \omega_f}$$

$$S(s) = \frac{\omega_s}{s + \omega_s}$$

$$D_R = \frac{K_{p1}}{s^2}$$

$$D_1 = \frac{K_{11} + K_{12}s^2}{s^2 + 2\zeta_1\omega_1 s + \omega_1{}^2}$$

$$D_2 = \frac{K_{21} + K_{22}s^2}{s^2 + 2\zeta_2\omega_2 s + \omega_2{}^2}$$

See table 3 for list of coefficients used.

Error coefficients.- The error coefficients a_1 and a_2 are a measure of the influence of errors in the modal data on the dynamic response of the system. If there are no modal errors, these coefficients are zero and, consequently, the bending motion is completely filtered out. The determination of the extent of the influence of modal errors on the stability of the controlled system requires that equations (49) and (50) be evaluated. A digital computer program was formulated to evaluate these equations for a range of assumed errors in the modal slopes. The error coefficients which are tabulated as a function of the percentage errors in a pair of modal slopes in table 4 are typical of the values obtained. The error coefficients corresponding to the errors in any other group of modal slopes are related by equation (42) to the δq_{pj} coefficients shown in table 2. In computing these coefficients, it was assumed that the sensors were located at distances of 19.3, 48.1, and 69.7 meters from the gimbal axis. A flight time corresponding to the condition of maximum dynamic pressure was also assumed. The influence of the error coefficients on the dynamic response of the system is given by equation (53). This equation was evaluated by using the tabulated values of the error coefficients as input to a second digital computer program which was devised to provide frequency response and root-locus data. From the stability point of view, the effect of errors in the modal data may be thought of as changing a system with ideal (cancellation) compensation into one with unideal compensation, the poles of the compensator being the bending mode poles. In the ideal case, when modal errors are absent, the poles and zeros of the compensator occupy the same locations in the complex plane. However, when modal errors are introduced, the zeros of the compensator move away from the poles. For example, if the modal errors are such that a given error coefficient a_i assumes a negative value, the zeros of the corresponding compensator move away from the bending mode pole in the direction of increasing complex frequency. Alternatively, if the modal errors are such that an error coefficient assumes a positive value, the zeros of the corresponding compensator move closer to the origin of the complex plane. The separation of the poles and zeros of the compensator with modal errors introduces the possibility of an unstable

condition when the loop is closed. Examination of the tabulated error coefficients reveals that for the sensor locations and flight time chosen, these coefficients can have the same or opposite sign, depending on which modal slope or group of modal slopes are in error; and also on whether the modal errors are positive or negative. Since the results contained in table 4 have all possible combinations of sign, these values of the error coefficients were used in conjunction with equation (53) to construct the root-locus plots shown in figures 5 through 18.

Error coefficients both positive.- In figures 5 through 9 it is seen that if there is a negative error in mode 1 at sensor location 1, and a negative error in mode 2 at sensor location 1, then both error coefficients are positive. In this case, both bending loci lie entirely in the left-half plane, indicating that both bending modes are stable for all magnitudes of modal errors.

Error coefficients a_1 positive and a_2 negative.- This combination of error coefficient signs is produced by a negative error in mode 1 at sensor 1, and a negative error in mode 2 at sensor 2. Figures 10 through 12 show that in these circumstances, the root-locus for the first bending mode lies entirely in the left-half plane, indicating that in the presence of such modal errors, the first bending mode is always stable. Although the locus for the second bending mode lies initially in the left-half plane, the figures show that as the error in the second mode is increased negatively at sensor 2, the stability of the second bending mode is degraded. Further increases of modal errors in the sense indicated may cause the second bending mode to become unstable.

Error coefficients a_1 negative and a_2 positive.- A positive error in mode 1 at sensor 1 and a positive error in mode 2 at sensor 2 produces an error coefficient a_1 which is negative and an error coefficient a_2 which is positive. As can be seen from figures 13 through 15 the root-locus for the second bending mode lies entirely in the left-half plane, indicating that the second bending mode is always stable in the presence of such modal errors. In this case the locus for the first bending mode, which initially lies in the left-half plane, moves into the right-half plane as the modal errors are increased. Hence, modal errors of this kind can produce an instability in the first bending mode.

Error coefficients both negative.- If both the first and the second bending modes have positive errors at sensor 1, both error coefficients assume negative values. Although both bending modes are stable for small errors in the modal data, the presence of modal errors of this type degrades the stability of both bending modes. If modal errors are sufficiently large, both bending modes become unstable. Examination of figures 16 through 18, however, reveals that for the nominal range of gain considered the first bending mode is more sensitive to modal errors than the second.

For the sensor locations and the flight time chosen, it is immediately evident that the system is stable for small percentage errors in the modal data. However, it is seen that if the error in a given modal slope or group of modal slopes is such that an error coefficient $a_i (i=1,2)$ assumes a positive value, such modal errors have a stabilizing influence on the corresponding mode i; whereas, if the modal errors are such that an error coefficient

a_i assumes a negative value, the errors will have a destabilizing influence on the corresponding mode i. This suggests that an attempt be made to bias the nominal values of the modal slopes in such a way as to insure that the error coefficients are always positive. Examination of the tabulated data reveals that it is possible to do this. For the case considered in this report, both error coefficients can be made positive by assigning a negative bias to modal slopes ψ_{11}, ψ_{21}, ψ_{12} and a positive bias to the slopes ψ_{31}, ψ_{22}, and ψ_{32}. This is equivalent to the use of structural feedback to stabilize the bending modes in the presence of errors in the modal data.

CONCLUDING REMARKS

A method has been devised for extracting rigid-body motion from the total motion of a flexible body. The method, which does not rely on the relative frequencies of the closed-loop rigid-body control mode and the elastic modes as conventional filters do, is well adapted to situations where a flexible-body frequency coincides with, or differs only slightly, from the control mode frequency.

An analysis of the effects of modal errors on motion displays of a typical launch vehicle indicates that when the amplitude of the rigid-body pitch attitude is greater than or equal to the amplitude of the bending motion at the nose of the vehicle, the error in the pitch-attitude display will always be less than 16 percent if the modal slope errors do not exceed either +50 percent or -50 percent.

An analysis of the influence of modal errors on the stability of the closed-loop system indicates that certain combinations of modal errors tend to degrade stability of at least one of the bending modes; whereas, other combinations of modal errors tend to enhance bending mode stability. For modal errors of 10 percent or less, and those combinations of modal errors that tend to degrade stability, no instability occurred in either mode when the loop was closed with nominal gain. The results indicate, however, that for the nominal range of gain considered the first bending mode is more sensitive to errors in the modal data than the second and, presumably, higher bending modes.

It has been shown that when the error coefficients are positive, stability is maintained without degradation. This suggests that an attempt be made to bias the nominal value of the modal slopes in such a way as to ensure that the error coefficients are always positive. Examination of the tabulated data reveals that it is possible to do this for the range of modal error considered in this report. This is equivalent to the use of structural feedback to stabilize the bending modes in the presence of errors in the modal data.

It is not claimed that the results of the error analysis are complete. The assumption has been made that the errors in each group of modal slopes are always in the same direction, that is, all positive errors or all negative errors. It is more probable that one or more members of any group of modal slopes will be subject to errors in one direction; while the remaining slopes

of the group will have errors of opposite sign. However, the error analysis given is felt to provide a basis for the assessment of the effects of the modal error distribution.

Ames Research Center
National Aeronautics and Space Administration
Moffett Field, Calif., June 28, 1965

APPENDIX A

ACCELERATIONS IN THE PITCH PLANE

Let A_i denote the output of an accelerometer which has its sensitive axis in the plane of the motion and perpendicular to the longitudinal axis of the vehicle. If second-order quantities are neglected, and if $(x_i - x_{cg})$ is the distance of the ith accelerometer from the center of gravity of the vehicle, then the linear acceleration at the ith accelerometer may be obtained by differentiating equation (14) twice with respect to time

$$A_i = \left[\ddot{q}_T + (x_i - x_{cg})\ddot{q}_p + \sum_{j=1}^{n} \varphi_{ij}\ddot{q}_j \right] \tag{A1}$$

where $\ddot{q}_T$ is the component of rigid-body acceleration in the translational mode, and $\varphi_{ij} = \varphi_j(x_i)$ is the modal displacement in the jth mode at sensor location i.

Because of the fact that the rigid-body acceleration has two components, the number of sensors required to provide sufficient information for determining the rigid-body components and the bending components is (n+2). Hence, the equations to be solved are

$$\begin{pmatrix} A_1 \\ A_2 \\ \cdot \\ \cdot \\ \cdot \\ A_n \\ A_{n+1} \\ A_{n+2} \end{pmatrix} = \begin{pmatrix} 1 & (x_1 - x_{cg}) & \varphi_{11} & \varphi_{12} & \cdots & \varphi_{1n} \\ 1 & (x_2 - x_{cg}) & \varphi_{21} & \varphi_{22} & \cdots & \varphi_{2n} \\ \cdot & \cdot & \cdot & \cdot & \cdots & \cdot \\ \cdot & \cdot & \cdot & \cdot & \cdots & \cdot \\ \cdot & \cdot & \cdot & \cdot & \cdots & \cdot \\ 1 & (x_n - x_{cg}) & \varphi_{n1} & \varphi_{n2} & \cdots & \varphi_{nn} \\ 1 & (x_{n+1} - x_{cg}) & \varphi_{n+1,1} & \varphi_{n+1,2} & \cdots & \varphi_{n+1,n} \\ 1 & (x_{n+2} - x_{cg}) & \varphi_{n+2,1} & \varphi_{n+2,2} & \cdots & \varphi_{n+2,n} \end{pmatrix} \begin{pmatrix} \ddot{q}_T \\ \ddot{q}_p \\ \cdot \\ \cdot \\ \cdot \\ \cdot \\ \cdot \\ \ddot{q}_n \end{pmatrix} \tag{A2}$$

This matrix equation can be solved to determine the unknown rigid-body accelerations and the n bending accelerations as functions of the measured outputs from the sensors and known modal data. To render these equations more

manageable, it is convenient to rewrite them in abbreviated form as follows

$$[A] = [\varphi][\ddot{Q}] \tag{A3}$$

where [A] is a column vector of measured accelerations, and $[\ddot{Q}]$ is a column vector consisting of the translational acceleration, the pitching acceleration, and the n bending accelerations. To simplify the formulation, the first two columns of the matrix $[\varphi]$ are redefined as follows

$$[\varphi] = \begin{pmatrix} \varphi_{1T} & \varphi_{1P} & \varphi_{11} & \cdots & \varphi_{1n} \\ \varphi_{2T} & \varphi_{2P} & \varphi_{21} & \cdots & \varphi_{2n} \\ \varphi_{3T} & \varphi_{3P} & \varphi_{31} & \cdots & \varphi_{3n} \\ \cdot & \cdot & \cdot & \cdots & \cdot \\ \cdot & \cdot & \cdot & \cdots & \cdot \\ \cdot & \cdot & \cdot & \cdots & \cdot \\ \varphi_{n+1,T} & \varphi_{n+1,P} & \varphi_{n+1,1} & \cdots & \varphi_{n+1,n} \\ \varphi_{n+2,T} & \varphi_{n+2,P} & \varphi_{n+2,1} & \cdots & \varphi_{n+2,n} \end{pmatrix} \tag{A4}$$

where

$$\varphi_{iT} = 1$$

and

$$\varphi_{iP} = (x_i - x_{cg}) \qquad i = 1,2, \ldots ,n+2$$

The column vector of unknown acceleration components is obtained from equation (A3) in the form

$$[\ddot{Q}] = [\varphi]^{-1}[A] \tag{A5}$$

where the inverse of the matrix $[\varphi]$ is given by

$$[\varphi]^{-1} = \frac{1}{\Delta_A}\begin{pmatrix} \Phi_{1T} & \Phi_{2T} & \cdots & \Phi_{n+1,T} & \Phi_{n+2,T} \\ \Phi_{1P} & \Phi_{2P} & \cdots & \Phi_{n+1,P} & \Phi_{n+2,P} \\ \Phi_{11} & \Phi_{21} & \cdots & \Phi_{n+1,1} & \Phi_{n+2,1} \\ \Phi_{12} & \Phi_{22} & \cdots & \Phi_{n+1,2} & \Phi_{n+2,2} \\ \cdot & \cdot & \cdots & \cdot & \cdot \\ \cdot & \cdot & \cdots & \cdot & \cdot \\ \cdot & \cdot & \cdots & \cdot & \cdot \\ \Phi_{1n} & \Phi_{2n} & \cdots & \Phi_{n+1,n} & \Phi_{n+2,n} \end{pmatrix} \tag{A6}$$

where Φ_{ij} is the cofactor of the corresponding element in the matrix $[\varphi]$ and Δ_A is the determinant of $[\varphi]$.

Rigid-body translational acceleration.- Upon substitution from equation (A6) in equation (A5), the rigid-body translational acceleration is obtained in the form of the series

$$\ddot{q}_T = \frac{1}{\Delta_A}\left(\Phi_{1T}A_1 + \Phi_{2T}A_2 + \cdots \Phi_{n+1,T}A_{n+1} + \Phi_{n+2,T}A_{n+2}\right)$$

that is

$$\ddot{q}_T = \frac{1}{\Delta_A}\sum_{i=1}^{n+2} \Phi_{iT}A_i \tag{A7}$$

The coefficient of A_i in equation (A7) will be denoted by $P_{Ti}(\varphi)$ and is the function to be used in processing the output from an accelerometer located at x_i on the flexible structure, in order to obtain the rigid-body translational acceleration. Equation (A7) shows that when the output from each accelerometer is processed in this way, the sum of the processed outputs gives the rigid-body translational acceleration (see fig. 19). In terms of the processing functions $P_{Ti}(\varphi)$, equation (A7) may be rewritten as follows

$$\ddot{q}_T = \sum_{i=1}^{n+2} P_{Ti}(\varphi)A_i \tag{A8}$$

where

$$P_{Ti}(\varphi) = \frac{\Phi_{iT}}{\Delta_A} \tag{A9}$$

Rigid-body pitching acceleration.- Equations (A5) and (A6) give the rigid-body pitching acceleration in the form of the series

$$\ddot{q}_p = \frac{1}{\Delta_A}\left(\Phi_{1P}A_1 + \Phi_{2P}A_2 + \cdots + \Phi_{n+1,P}A_{n+1}\Phi_{n+2,P}A_{n+2}\right)$$

that is

$$\ddot{q}_p = \frac{1}{\Delta_A}\sum_{i=1}^{n+2}\Phi_{iP}A_i \tag{A10}$$

The coefficient of A_i in equation (A10) is the function to be used in processing the output from an accelerometer located at x_i in order to obtain the rigid-body pitching acceleration. This processing function will be denoted by $P_{pi}(\varphi)$. Equation (A10) shows that the sum of the processed outputs gives the rigid-body pitching acceleration. In terms of the processing functions $P_{pi}(\varphi)$, equation (A10) may be rewritten in the following form

$$\ddot{q}_p = \sum_{i=1}^{n+2} P_{pi}(\varphi)A_i \tag{A11}$$

where

$$P_{pi}(\varphi) = \frac{\Phi_{iP}}{\Delta_A} \tag{A12}$$

Similarly, by using equation (A6) to obtain the appropriate processing functions, it is possible to determine modal accelerations from which may be derived modal rates and modal displacements. These quantities may be used in a feedback loop to supplement attitude and attitude rate information. An interesting application which suggests itself is the use of structural feedback to suppress or attenuate flexible body motion by augmenting the generalized mass, the structural damping, and the structural stiffness. See figure 20.

REFERENCES

1. Evans, Walter R.; and Jerger, Joseph H.: Autopilot Signals Free of Bending Modes Despite Structural Uncertainties. A.R.S. Guidance, Control, and Navigation Conference, Stanford Univ., Stanford, California, Aug. 7-9, 1961.

2. Zaborszy, John; Luedde, William J.; and Wendl, Michael J.: New Flight Control Techniques for a Highly Elastic Booster. ASD Tech. Rep. 61-231.

3. Prince, L. T.: New Flight Control System Techniques for a Highly Elastic Booster. ASD Tech. Rep. 61-174 or MA Aero Report 2491-TR1.

4. Timoshenko, Stephen; and Young, D. H.: Vibration Problems in Engineering. Third ed., D. Van Nostrand Co., Inc., New York, 1955.

5. Lukens, David R.; Schmitt, Alfred F.; and Broucek, George T.: Approximate Transfer Functions for Flexible Booster and Autopilot Analysis. WADD TR 61-93.

6. Bisplinghoff, Raynold L.; Holt, Ashley; and Halfman, Robert L.: Aeroelasticity. Addison-Wesley Pub. Co., Inc., Cambridge, Mass., 1955.

7. Kachigan, K.: The General Theory and Analysis of a Flexible Bodied Missile with Autopilot Control. Rep. ZU-7-048 (Contract No. AF04(645)-4), CONVAIR, Nov. 11, 1955.

8. Young, Dana: Generalized Missile Dynamics Analysis. II - Equations of Motion. GM TR-0165-00359, Space Tech. Labs., The Ramo-Wooldridge Corp., Apr. 7, 1958.

TABLE I.- BENDING MODE DATA

t = 80 sec				
x, meters	$*\varphi_1(x)$	$\psi_1(x)$	$*\varphi_2(x)$	$\psi_2(x)$
0.1	1.1219	0.05065	1.1585	0.06504
2.5	1.0000	.05097	1.0000	.06693
4.9	.8773	.05122	.8373	.06837
7.3	.7543	.05151	.6728	.06985
9.7	.6290	.05283	.4969	.07623
12.1	.5012	.05346	.3099	.07843
14.5	.3736	.05284	.1254	.07510
16.9	.2449	.05386	-.06336	.07976
19.3	.1179	.05192	-.2431	.06968
21.7	-.003921	.04955	-.3947	.05402
24.1	-.1141	.04493	-.4790	.02767
26.5	-.2197	.04294	-.5284	.01334
28.9	-.3199	.04058	-.5429	-.000884
31.3	-.4151	.03867	-.5324	-.007722
33.7	-.5054	.03662	-.5063	-.01393
36.1	-.5909	.03604	-.4647	-.02850
38.5	-.6718	.03127	-.3838	-.03867
40.9	-.7406	.02625	-.2836	-.04463
43.3	-.7982	.02171	-.1686	-.05102
45.7	-.8446	.01690	-.03958	-.05626
48.1	-.8763	.008959	.09996	-.05935
50.5	-.8881	.001829	.2429	-.06033
52.9	-.8864	-.003258	.3897	-.06186
55.5	-.8727	-.008119	.5389	-.06227
57.7	-.8476	-.02174	.6878	-.06183
60.1	-.8090	-.02364	.8399	-.07291
62.5	-.7397	-.03391	1.0081	-.06786
64.9	-.6468	-.04356	1.1656	-.06302
67.3	-.5299	-.05408	1.3085	-.05554
69.7	-.3864	-.06559	1.5290	-.04374
72.1	-.2158	-.07636	1.5155	-.02809
74.5	-.02079	-.08593	1.5615	-.009608
76.9	.1957	-.09425	1.5607	.01032
79.3	.4306	-.1013	1.5119	.03027
81.7	.6809	-.1071	1.4160	.04946
84.1	1.0037	-.1430	1.1845	.1235
86.5	1.3616	-.1551	.8365	.1638
88.9	1.7457	-.1645	.4044	.1952
91.3	2.1338	-.1595	-.2044	.2263
93.7	2.5204	-.1624	-.6694	.2431
96.1	2.9174	-.1697	-1.23411	.2730
98.5	3.3323	-.1687	-1.9730	.2763
100.9	3.7321	-.1644	-2.6196	.2614
103.3	4.1197	-.1487	-3.2176	.2373

*Normalized to unity at gimbal point.

TABLE II.- DISPLAY ERRORS CALCULATED FOR GIVEN ERRORS IN MODAL SLOPES

Percentage error in modal slopes	Display error per degree of bending at the nose of the vehicle, in mode j		Percentage error in modal slopes	Display error per degree of bending at the nose of the vehicle, in mode j	
ψ_{11}	δq_{p1}	δq_{p2}	ψ_{12}	δq_{p1}	δq_{p2}
-50	-0.07568	0	-50	0	0.08178
-40	-.06005		-40		.06127
-30	-.04467		-30		.04324
-20	-.02954		-20		.02720
-10	-.01465		-10		.01288
0	0		0		0
10	.01442		10		-.01164
20	.02863		20		-.02221
30	.04261		30		-.03186
40	.05638		40		-.04071
50	.06994	↓	50	↓	-.04880
ψ_{21}	δq_{p1}	δq_{p2}	ψ_{22}	δq_{p1}	δq_{p2}
-50	-.00708	0	-50	0	-.04227
-40	-.00561		-40		-.03067
-30	-.00416		-30		-.02104
-20	-.00274		-20		-.01293
-10	-.00136		-10		-.00600
0	0		0		0
10	.00133		10		.00523
20	.00264		20		.00984
30	.00392		30		.01393
40	.00518		40		.01759
50	.00642	↓	50	↓	.02087
ψ_{31}	δq_{p1}	δq_{p2}	ψ_{32}	δq_{p1}	δq_{p2}
-50	.13490	0	-50	0	-.03041
-40	.09469		-40		-.02474
-30	.06327		-30		-.01888
-20	.03802		-20		-.01281
-10	.01731		-10		-.00652
0	0		0		0
10	-.01468		10		.00676
20	-.02728		20		.01378
30	-.03822		30		.01981
40	-.04781		40		.02865
50	-.05628	↓	50	↓	.03653
$\psi_{11}\psi_{12}$	δq_{p1}	δq_{p2}	$\psi_{11}\psi_{22}$	δq_{p1}	δq_{p2}
-50	-.10262	.08630	-50	-.05707	-.05993
-40	-.07586	.06380	-40	-.04963	-.04185
-30	-.05287	.04446	-30	-.03968	-.02717
-20	-.03292	.02769	-20	-.02765	-.01555
-10	-.01544	.01298	-10	-.01426	-.00662
0	0	0	0	0	0
10	.01374	-.01155	10	.01470	.00467
20	.02604	-.02190	20	.02954	.00771
30	.03712	-.03122	30	.04426	.00941
40	.04715	-.03965	40	.05871	.01001
50	.05627	-.04732	50	.07275	.00973
$\psi_{11}\psi_{32}$	δq_{p1}	δq_{p2}	$\psi_{12}\psi_{31}$	δq_{p1}	δq_{p2}
-50	-.06960	-.01946	-50	.16261	.07458
-40	-.05568	-.01761	-40	.10968	.05764
-30	-.04194	-.01478	-30	.07048	.04158
-20	-.02821	-.01094	-20	.04082	.02660
-10	-.01429	-.00604	-10	.01789	.01277
0	0	0	0	0	0
10	.01486	.00728	10	-.01420	-.01173
20	.03051	.01596	20	-.02560	-.02250
30	.04722	.02622	30	-.03481	-.03246
40	.06530	.03833	40	-.04237	-.04163
50	.08514	.05263	50	-.04855	-.05010
$\psi_{21}\psi_{22}$	δq_{p1}	δq_{p2}	$\psi_{21}\psi_{32}$	δq_{p1}	δq_{p2}
-50	-.01103	-.04568	-50	-.00955	-.02891
-40	-.00780	-.03245	-40	-.00720	-.02381
-30	-.00525	-.02187	-30	-.00511	-.01837
-20	-.00316	-.01323	-20	-.00316	-.01260
-10	-.00146	-.00607	-10	-.00147	-.00649
0	0	0	0	0	0
10	.00128	.00518	10	.00121	.00678
20	.00235	.00969	20	.00222	.01395
30	.00330	.01361	30	.00289	.02137
40	.00410	.01707	40	.00335	.02916
50	.00484	.02010	50	.00350	.03721

TABLE II.- DISPLAY ERRORS CALCULATED FOR GIVEN ERRORS IN MODAL SLOPES - Concluded

Percentage error in modal slopes	Display error per degree of bending at the nose of the vehicle, in mode j	
$\psi_{22}\psi_{31}$	δq_{p1}	δq_{p2}
-50	0.13470	-0.00051
-40	.09206	-.00995
-30	.06126	-.01159
-20	.03705	-.09418
-10	.01708	-.00523
0	0	0
10	-.01493	.00582
20	-.02818	.01188
30	-.04015	.01804
40	-.05097	.02415
50	-.06093	.03021
$\psi_{31}\psi_{32}$	δq_{p1}	δq_{p2}
-50	.11681	-.04880
-40	.08534	-.03569
-30	.05898	-.02465
-20	.03645	-.01521
-10	.01695	-.00712
0	0	0
10	-.01493	.00624
20	-.02818	.01176
30	-.04001	.01669
40	-.05057	.02115
50	-.06019	.02516
$\psi_{11}\psi_{12}\psi_{22}$	δq_{p1}	δq_{p2}
-50	-.08931	.04366
-40	-.06812	.03261
-30	-.04889	.02305
-20	-.03134	.01458
-10	-.01506	.00695
0	0	0
10	.01406	-.00636
20	.02717	-.01226
30	.03948	-.01770
40	.05104	-.02280
50	.06200	-.02756
$\psi_{11}\psi_{12}\psi_{32}$	δq_{p1}	δq_{p2}
-50	-.09321	.05608
-40	-.06967	.03877
-30	-.04936	.02528
-20	-.03134	.01471
-10	-.01506	.00641
0	0	0
10	.01412	-.00485
20	.02764	-.00830
30	.04075	-.01070
40	.05360	-.01201
50	.06637	-.01235
$\psi_{11}\psi_{21}\psi_{32}$	δq_{p1}	δq_{p2}
-50	-.08299	-.01736
-40	-.06530	-.01639
-30	-.04835	-.01416
-20	-.03194	-.01070
-10	-.01594	-.00598
0	0	0
10	.01594	.00528
20	.03201	.01606
30	.04855	.02638
40	.06557	.03839
50	.08346	.05230
$\psi_{11}\psi_{22}\psi_{32}$	δq_{p1}	δq_{p2}
-50	-.04963	-.08344
-40	-.04459	-.06245
-30	-.03658	-.04395
-20	-.02616	-.02752
-10	-.01385	-.01298
0	0	0
10	.01511	.01155
20	.03120	.02187
30	.04808	.03110
40	.06557	.03936
50	.08346	.04678

Percentage error in modal slopes	Display error per degree of bending at the nose of the vehicle, in mode j	
$\psi_{22}\psi_{32}$	δq_{p1}	δq_{p2}
-50	0	-0.08125
-40	↓	-.06098
-30		-.04307
-20		-.02713
-10		-.01285
0		0
10		.01163
20		.02225
30		.03194
40		.04083
50		.04901
$\psi_{11}\psi_{12}\psi_{21}$	δq_{p1}	δq_{p2}
-50	-0.10793	.08656
-40	-.08043	.06397
-30	-.05649	.04454
-20	-.03544	.02773
-10	-.01675	.01298
0	0	0
10	.01511	-.01155
20	.02884	-.02187
30	.04136	-.03114
40	.05286	-.03949
50	.06348	-.04711
$\psi_{11}\psi_{12}\psi_{31}$	δq_{p1}	δq_{p2}
-50	.00013	.08175
-40	.00215	.06119
-30	.00262	.04315
-20	.00222	.02718
-10	.00128	.01285
0	0	0
10	-.00141	-.01163
20	-.00289	-.02225
30	-.00444	-.03194
40	-.00592	-.04083
50	-.00740	-.04901
$\psi_{11}\psi_{21}\psi_{22}$	δq_{p1}	δq_{p2}
-50	-.07169	-.06452
-40	-.06005	-.04425
-30	-.04640	-.02823
-20	-.03147	-.01593
-10	-.01587	-.00670
0	0	0
10	.01580	.00464
20	.03134	.00759
30	.04640	.00919
40	.06093	.00973
50	.07485	.00940
$\psi_{11}\psi_{22}\psi_{31}$	δq_{p1}	δq_{p2}
-50	.01769	-.03675
-40	.01130	-.02815
-30	.00686	-.01997
-20	.00377	-.01256
-10	.00161	-.00594
0	0	0
10	-.00114	.00527
20	-.00202	.00999
30	-.00262	.01420
40	-.00309	.01799
50	-.00343	.02141
$\psi_{11}\psi_{31}\psi_{32}$	δq_{p1}	δq_{p2}
-50	.01715	-.03312
-40	.01110	-.02617
-30	.00686	-.01955
-20	.00383	-.01306
-10	.00161	-.00657
0	0	0
10	-.00114	.00670
20	-.00188	.01365
30	-.00237	.02082
40	-.00260	.02828
50	-.00261	.03603

TABLE III.- SYSTEM PARAMETERS

K_{12} = 0.04412 (dimensionless)

K_{22} = 0.042116 (dimensionless)

ω_f = 17.5 (1/sec)

ω_s = 30 (1/sec)

K_{p1} = 0.85 ($1/sec^2$)

K_{11} = 26.355 ($1/sec^2$)

K_{21} = 23.96 ($1/sec^2$)

ω_1 = 5.039 (1/sec)

ω_2 = 11.99 (1/sec)

ζ = 0.005 (dimensionless)

Kq_p = 0.7500 (dimensionless)

$K\dot{q}_p$ = 0.8025 (sec)

TABLE IV.- VALUES OF ERROR COEFFICIENTS USED TO CONSTRUCT ROOT-LOCUS PLOTS

Percentage error in modal slopes	Error coefficients		Percentage error in modal slopes	Error coefficients	
$\psi_{11}\psi_{12}$	a_1	a_2	$\psi_{11}\psi_{22}$	a_1	a_2
-50	0.01526	0.02048	-50	0.00849	-0.01422
-40	.01128	.01514	-40	.00738	-.00993
-30	.00786	.01055	-30	.00590	-.006447
-20	.004895	.00657	-20	.00411	-.00369
-10	.00229	.00308	-10	.00212	-.001571
0	0	0	0	0	0
10	-.002043	-.002741	10	-.002186	.001108
20	-.00387	-.00519	20	-.00439	.00183
30	-.00552	-.00741	30	-.00658	.002233
40	-.007011	-.009409	40	-.00873	.002376
50	-.00837	-.01123	50	-.01082	.00231

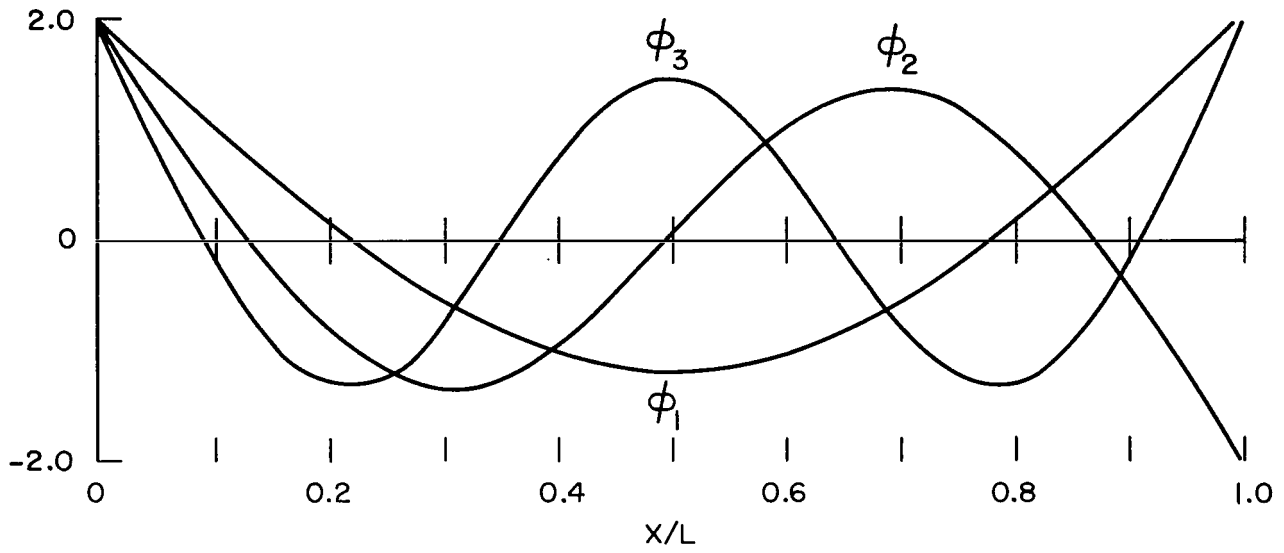

Figure 1.- The first three modal displacement functions for a uniform free-free beam.

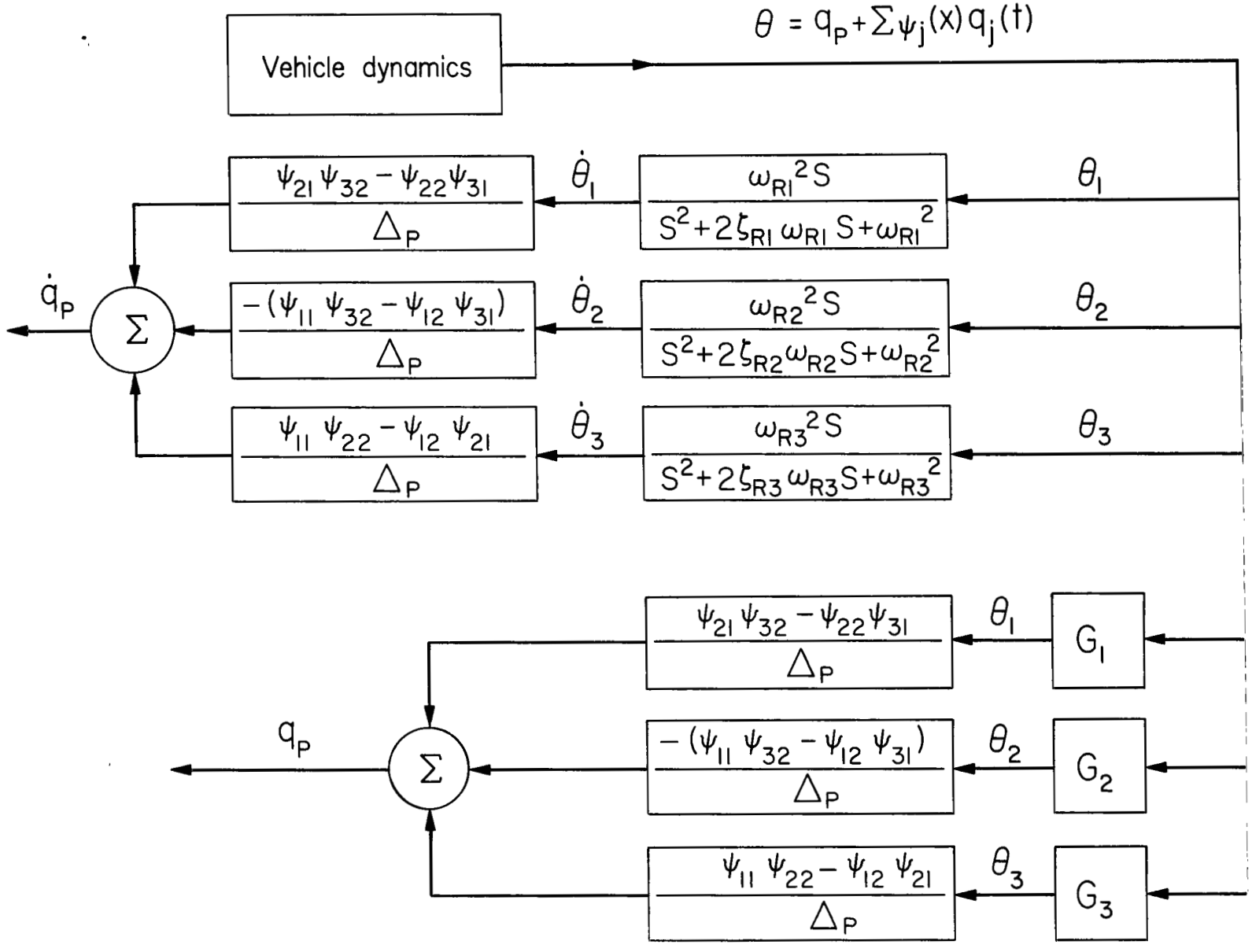

Figure 2.- Block diagram of system for processing attitude and attitude-rate information.

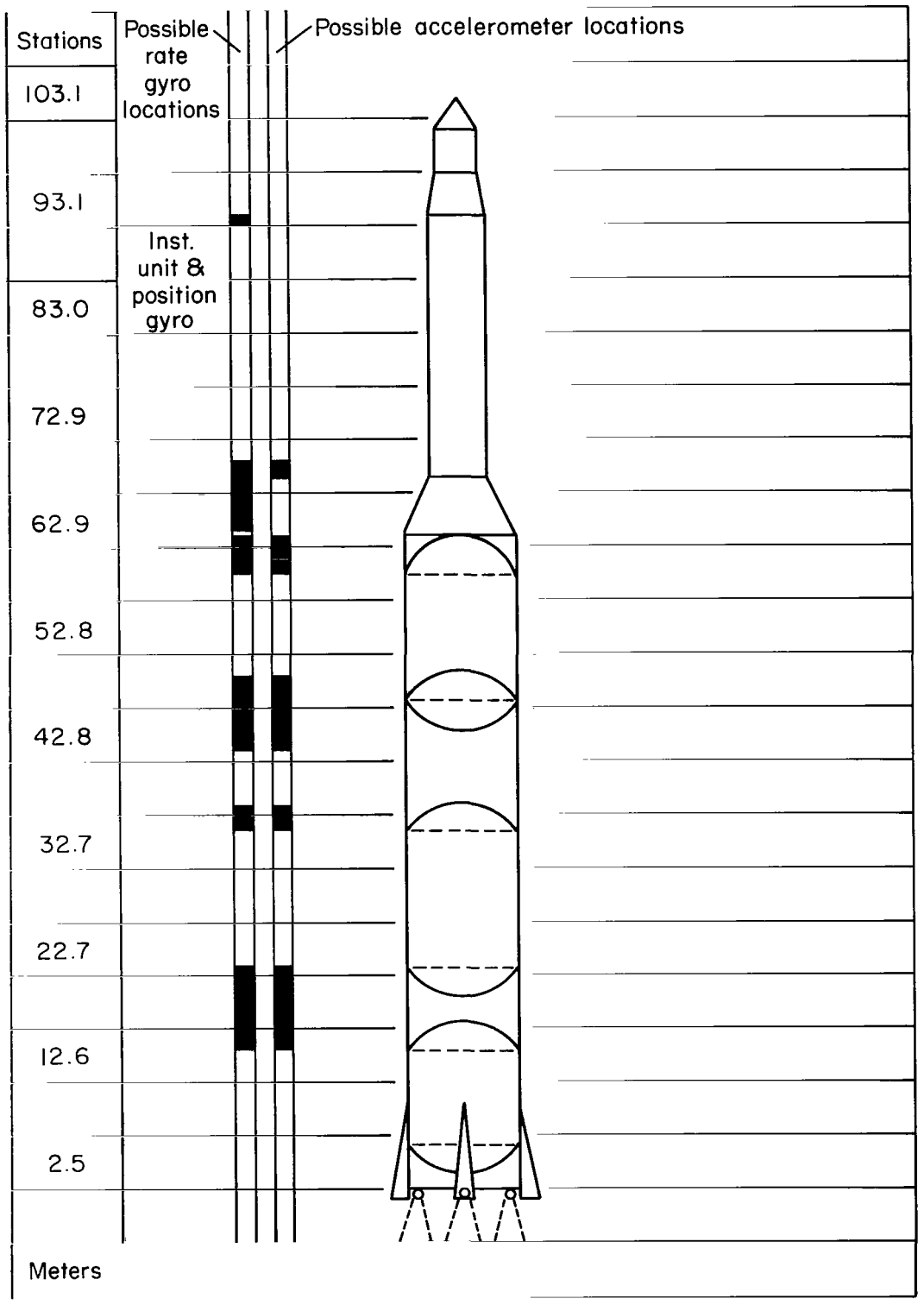

Figure 3.- Model vehicle configuration showing possible sensor locations.

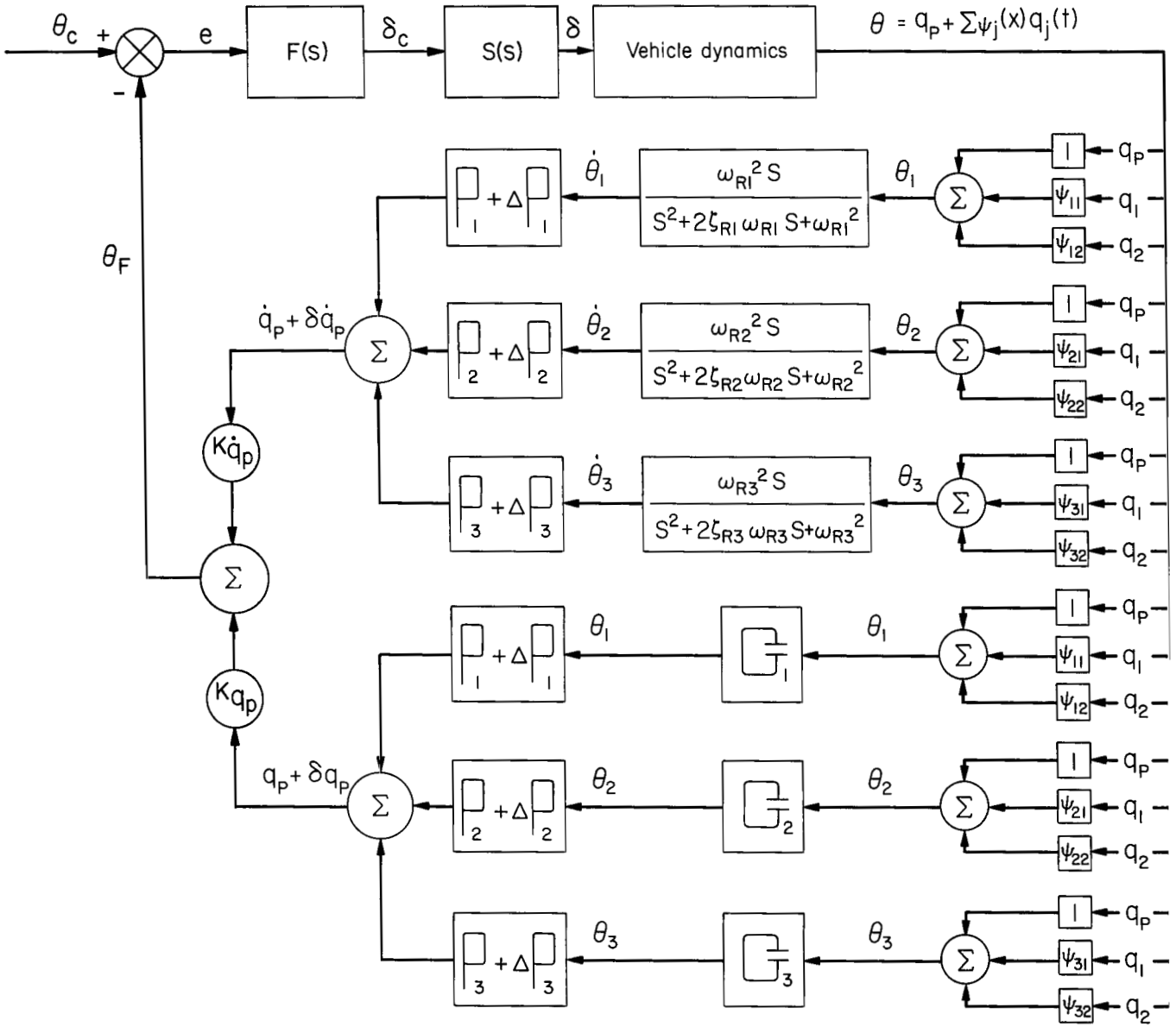

Figure 4.- Block diagram of the closed-loop system including the processing functions.

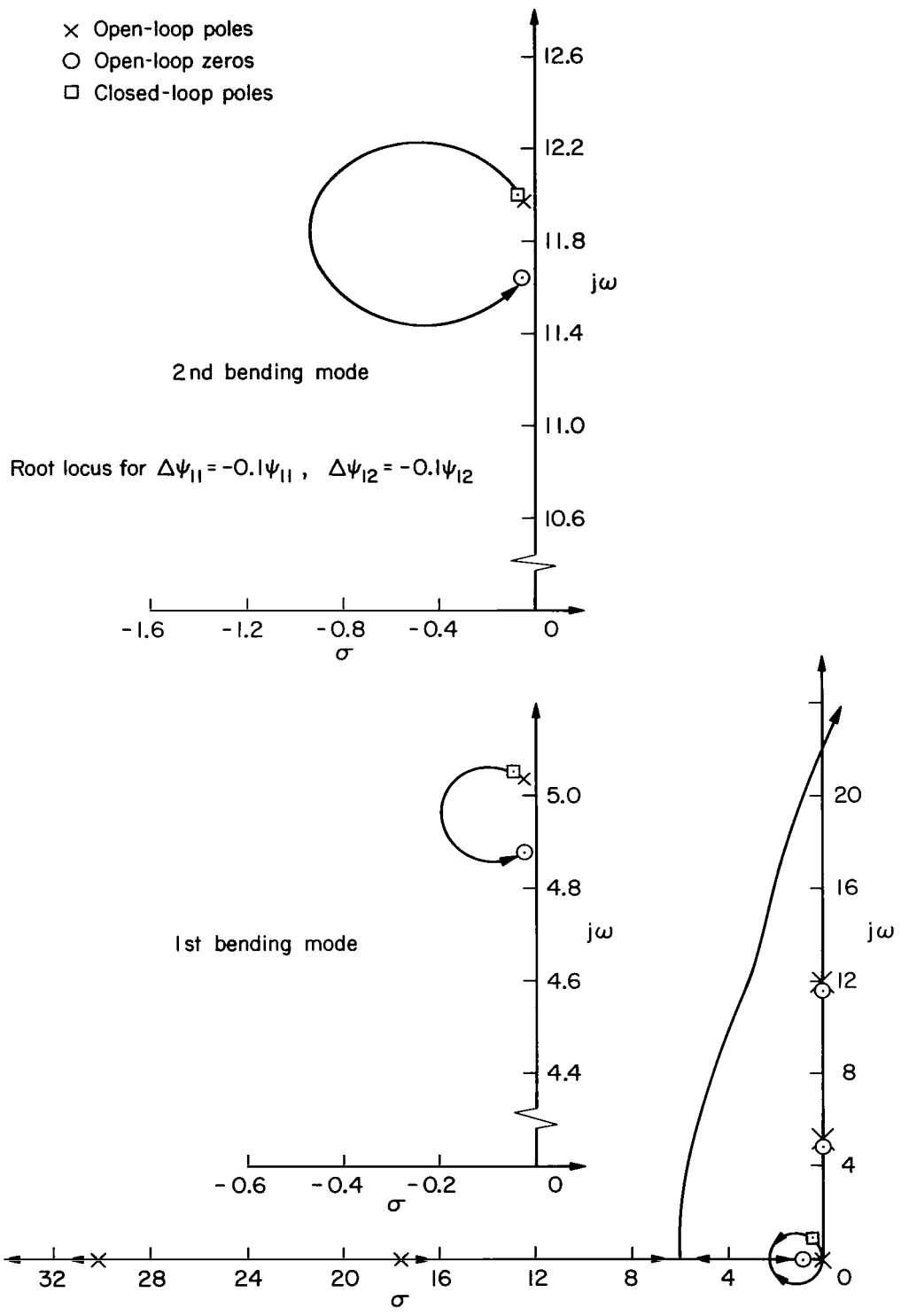

Figure 5.- Effect of modal errors on the root locus, both error coefficients positive, $a_1 = 0.002296$, $a_2 = 0.003081$.

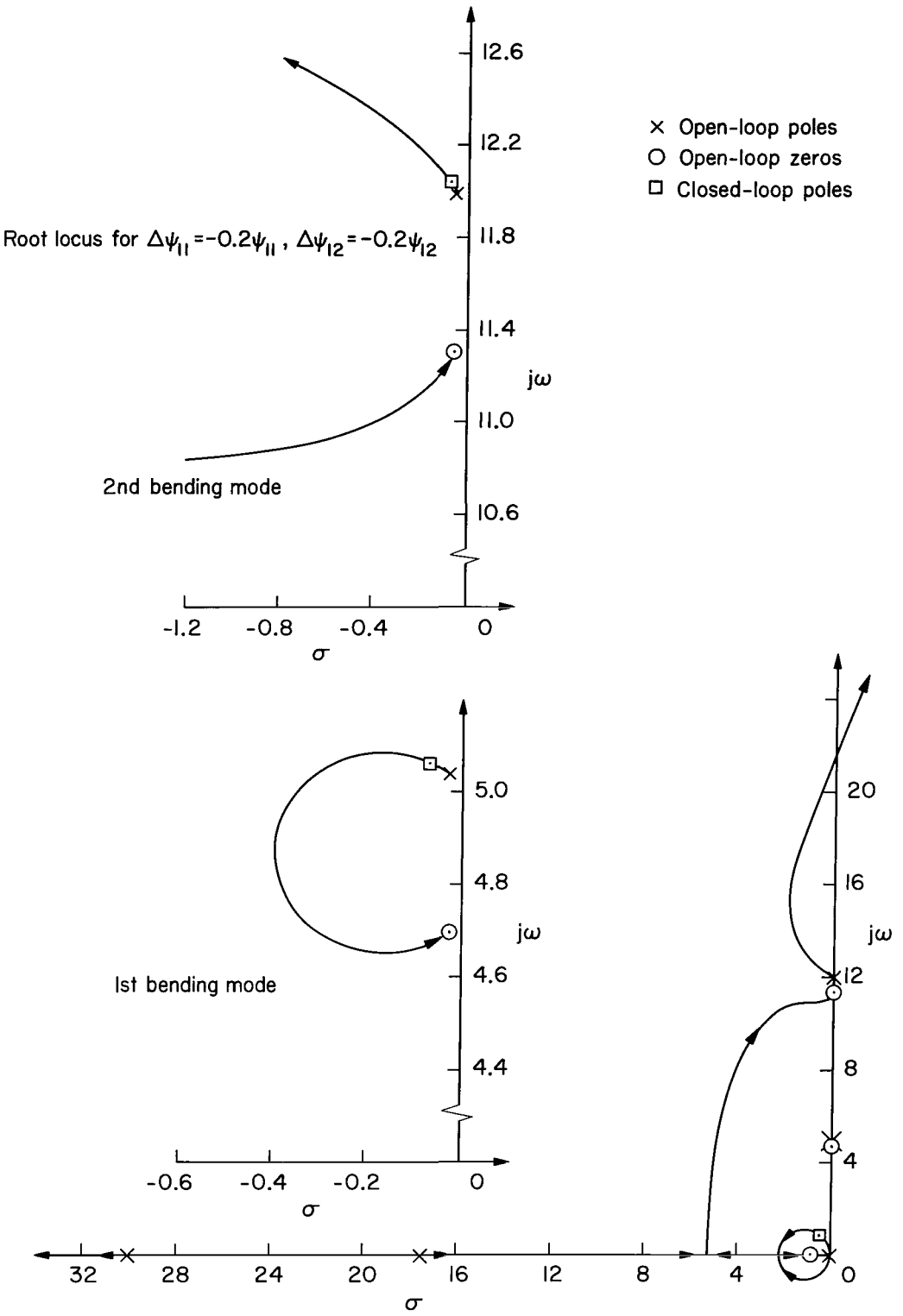

Figure 6.- Effect of modal errors on root locus, both error coefficients positive, $a_1 = 0.004895$, $a_2 = 0.00657$.

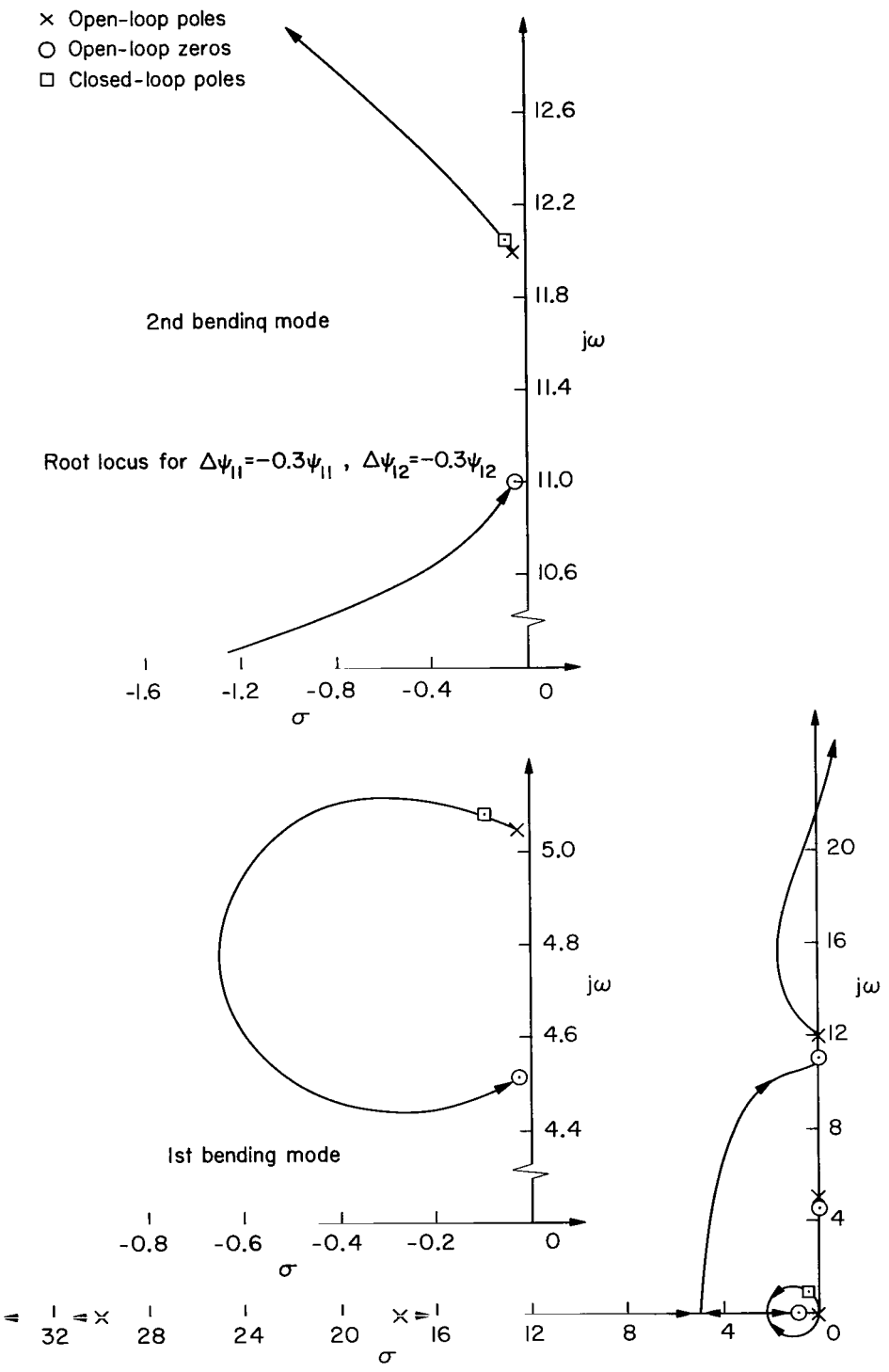

Figure 7.- Effect of modal errors on root locus, both error coefficients positive, $a_1 = 0.007862$, $a_2 = 0.01055$.

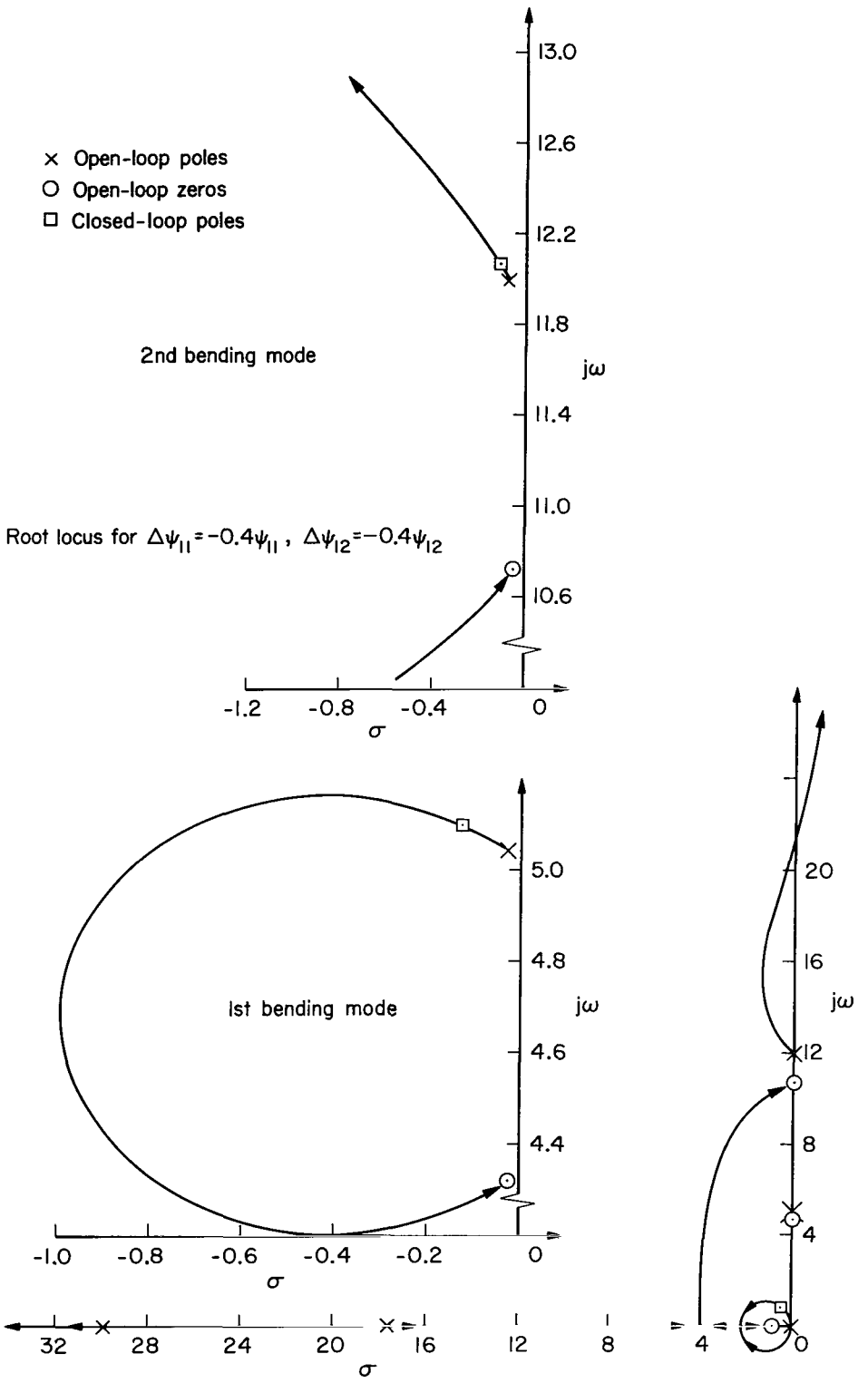

Figure 8.- Effect of modal errors on root locus, both error coefficients positive, $a_1 = 0.01128$, $a_2 = 0.01514$.

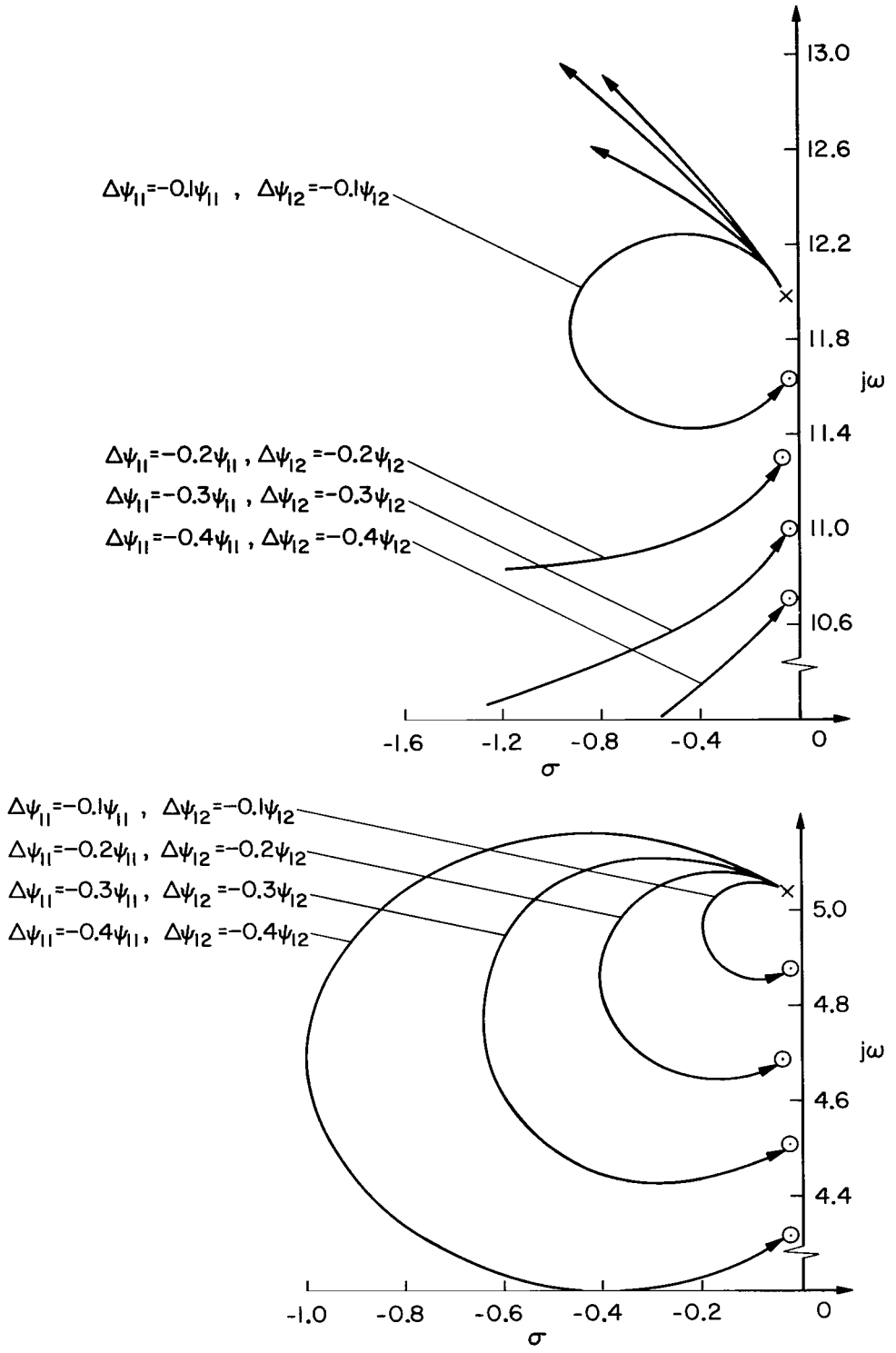

Figure 9.- Root-locus variations produced by negative error in mode 1 at sensor 1, and by negative error in mode 2 at sensor 1.

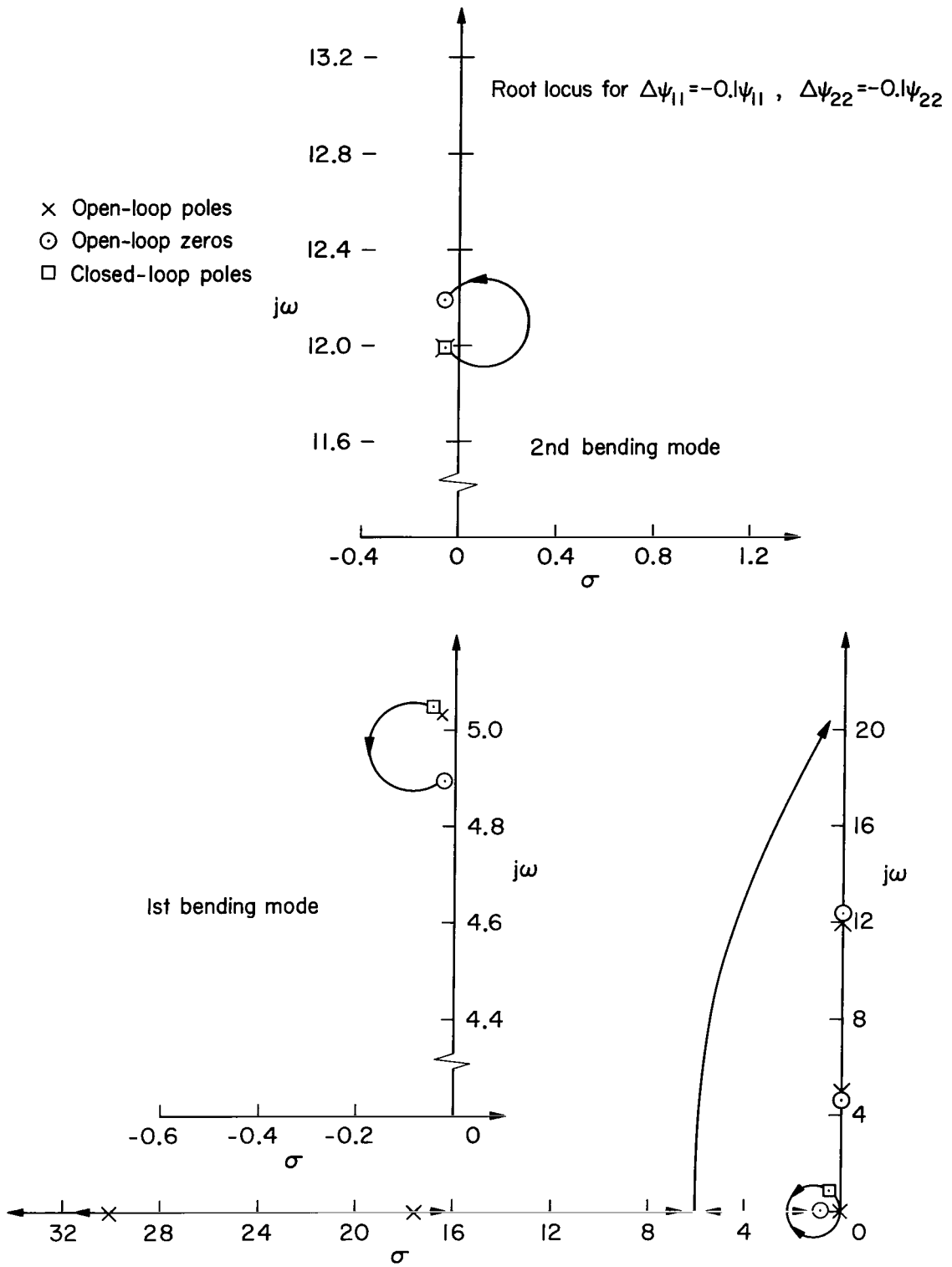

Figure 10.- Effect of modal errors on the root locus, error coefficients of opposite sign, a_1 = 0.00212, a_2 = -0.001571.

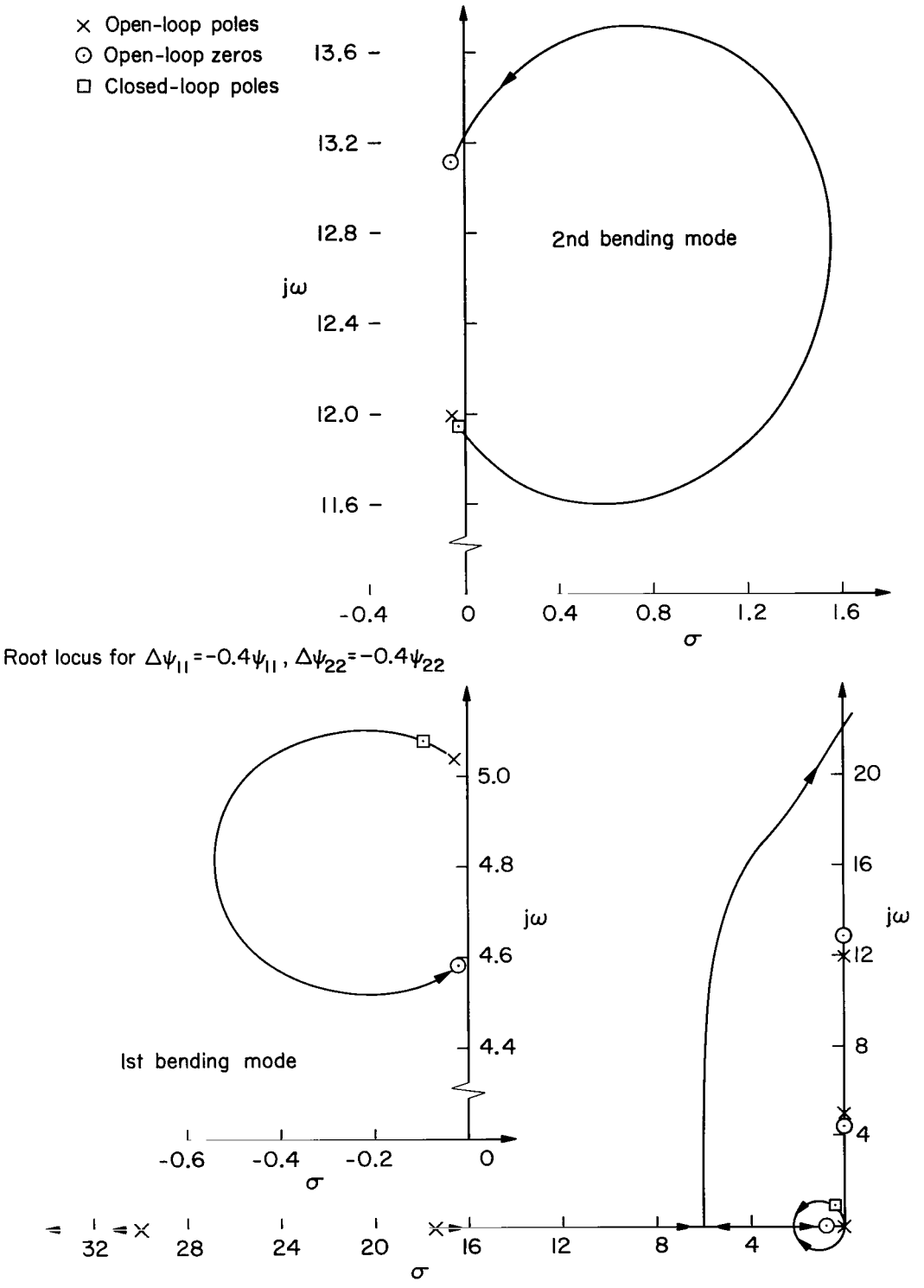

Figure 11.- Effect of modal errors on the root locus, error coefficients of opposite sign, $a_1 = 0.00738$, $a_2 = -0.00993$.

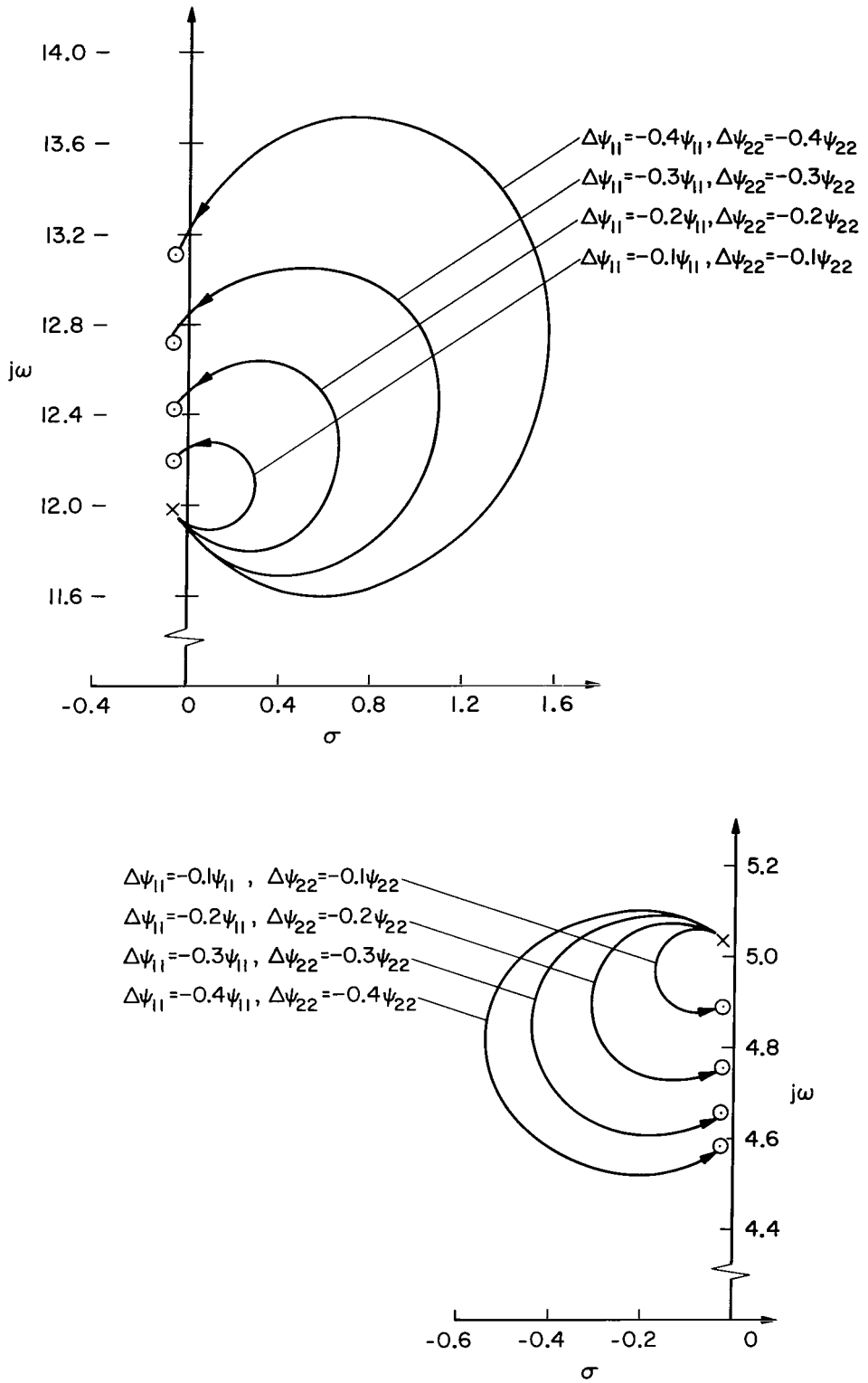

Figure 12.- Root-locus variations produced by negative error in mode 1 at sensor 1, and by negative error in mode 2 at sensor 2.

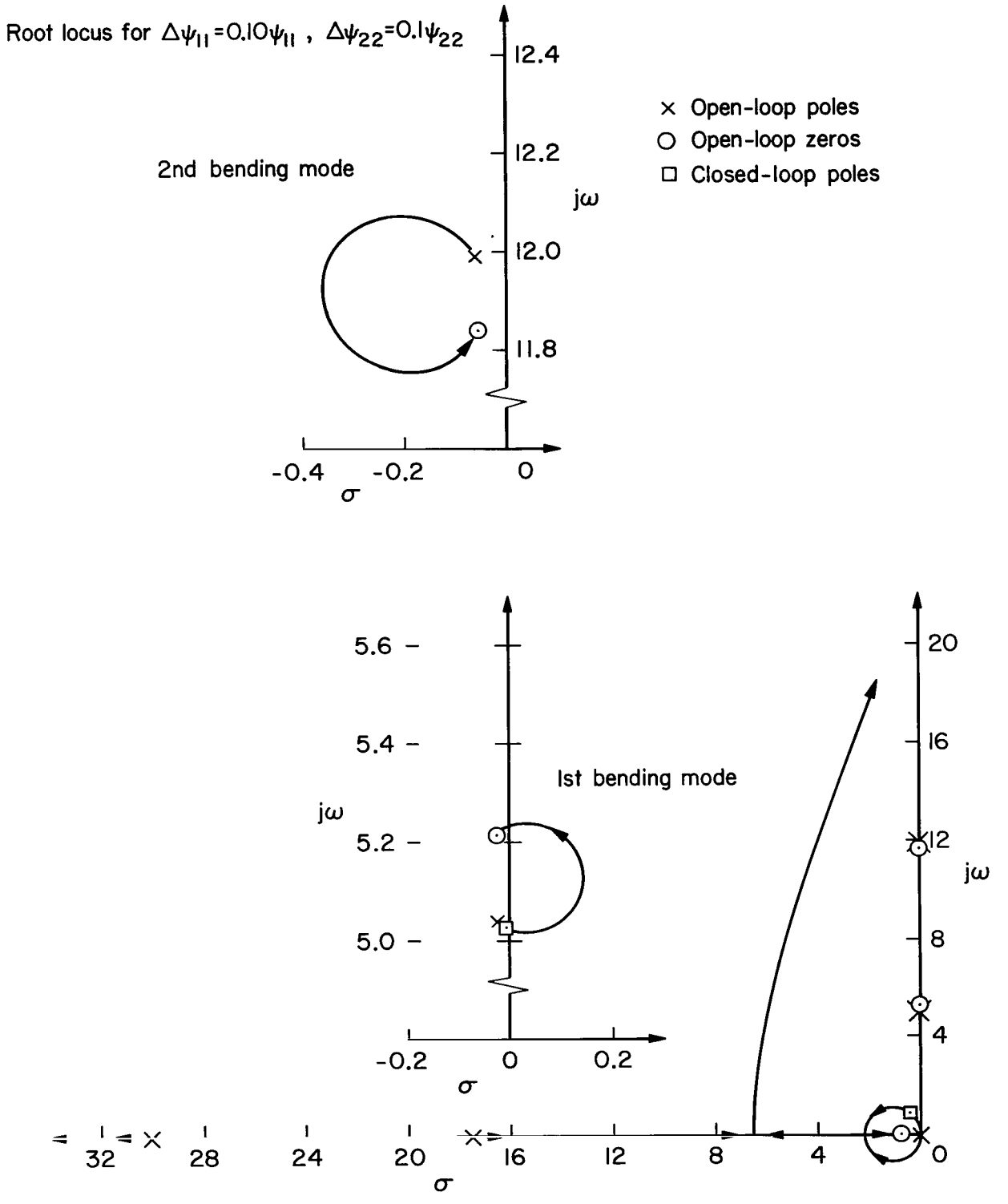

Figure 13.- Effect of modal errors on the root locus, error coefficients of opposite sign, $a_1 = -0.002186$, $a_2 = 0.001108$.

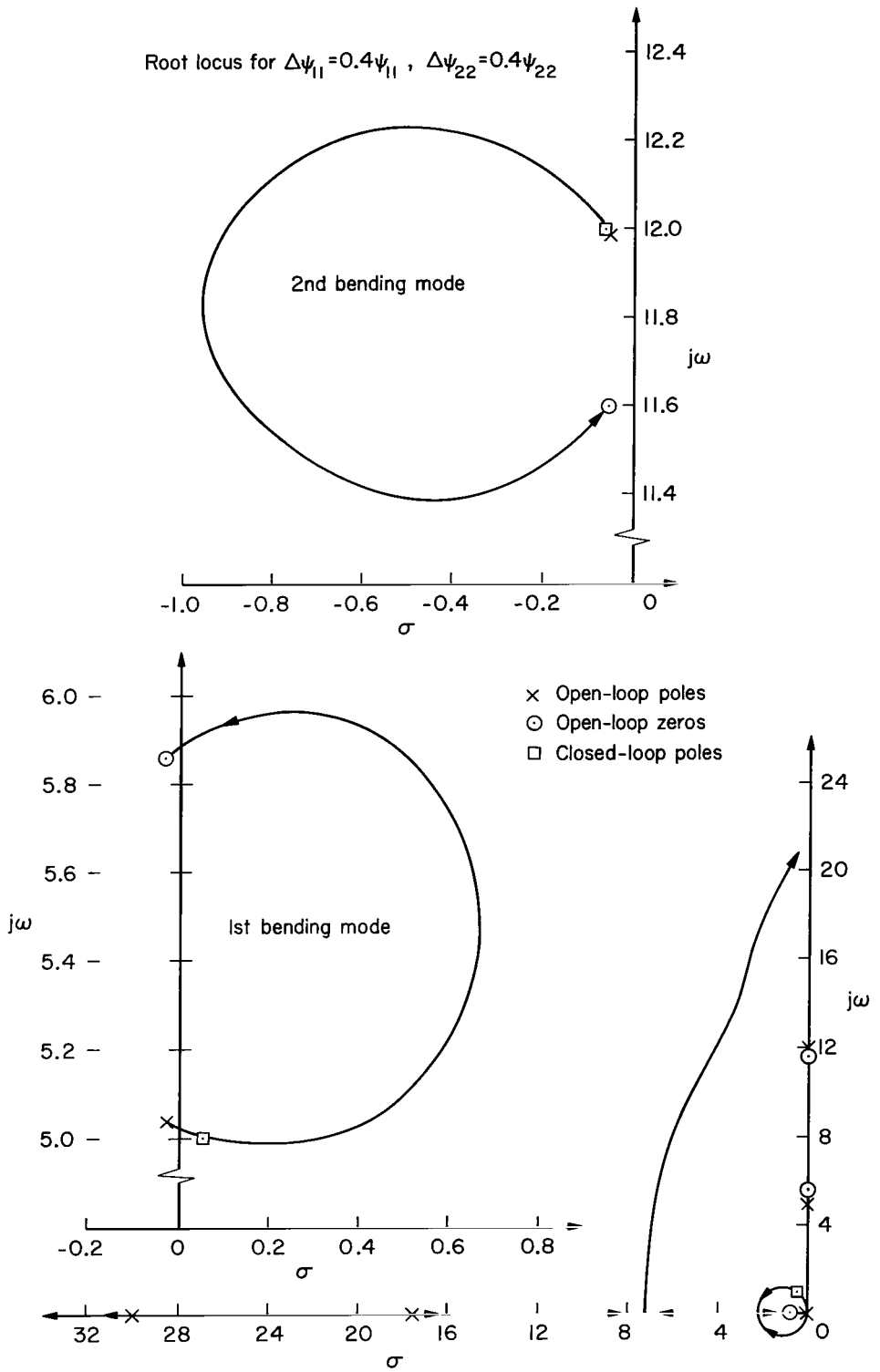

Figure 14.- Effect of modal errors on the root locus, error coefficients of opposite sign, $a_1 = -0.00873$, $a_2 = 0.002376$.

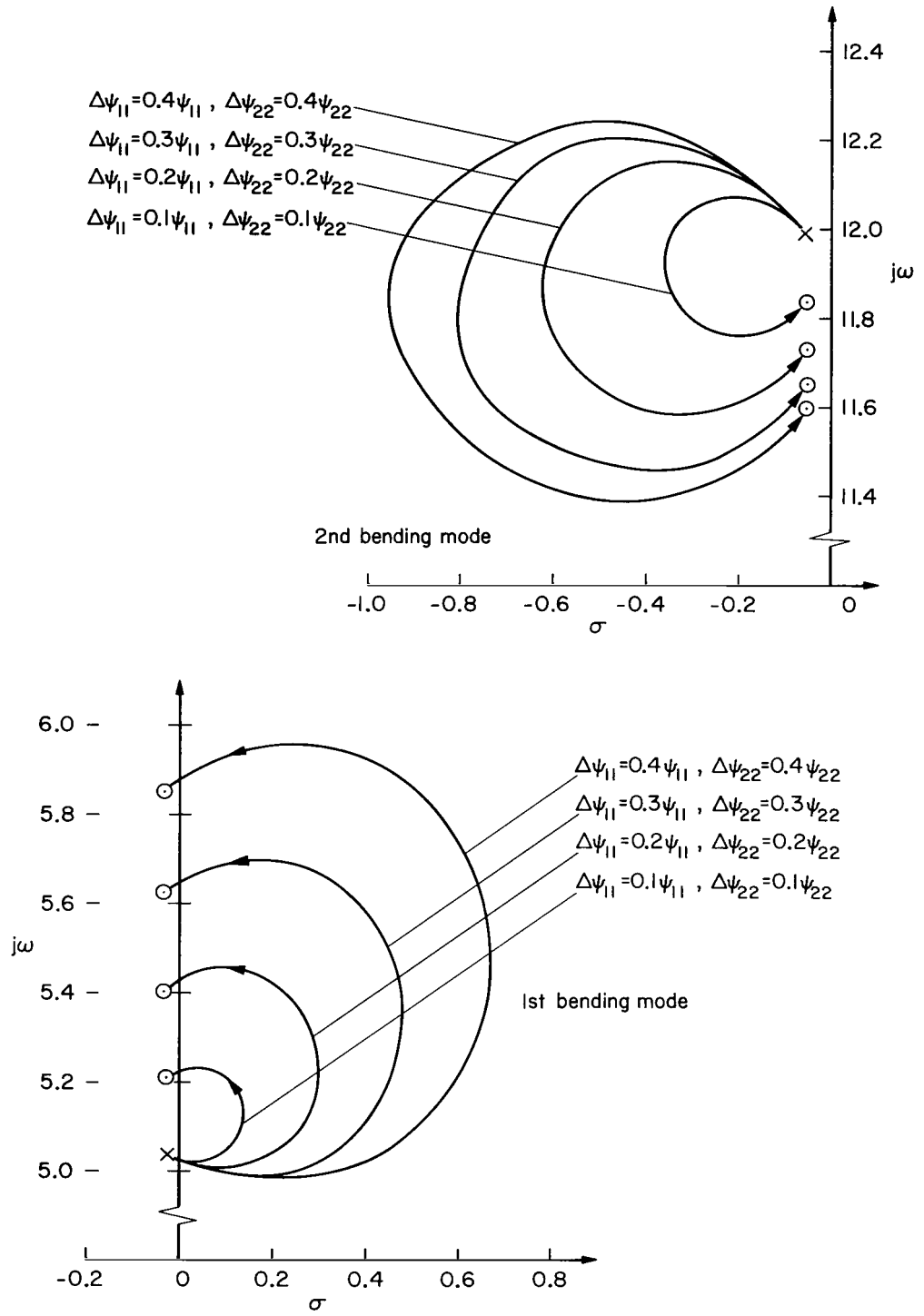

Figure 15.- Root-locus variations produced by positive error in mode 1 at sensor 1, and by positive error in mode 2 at sensor 2.

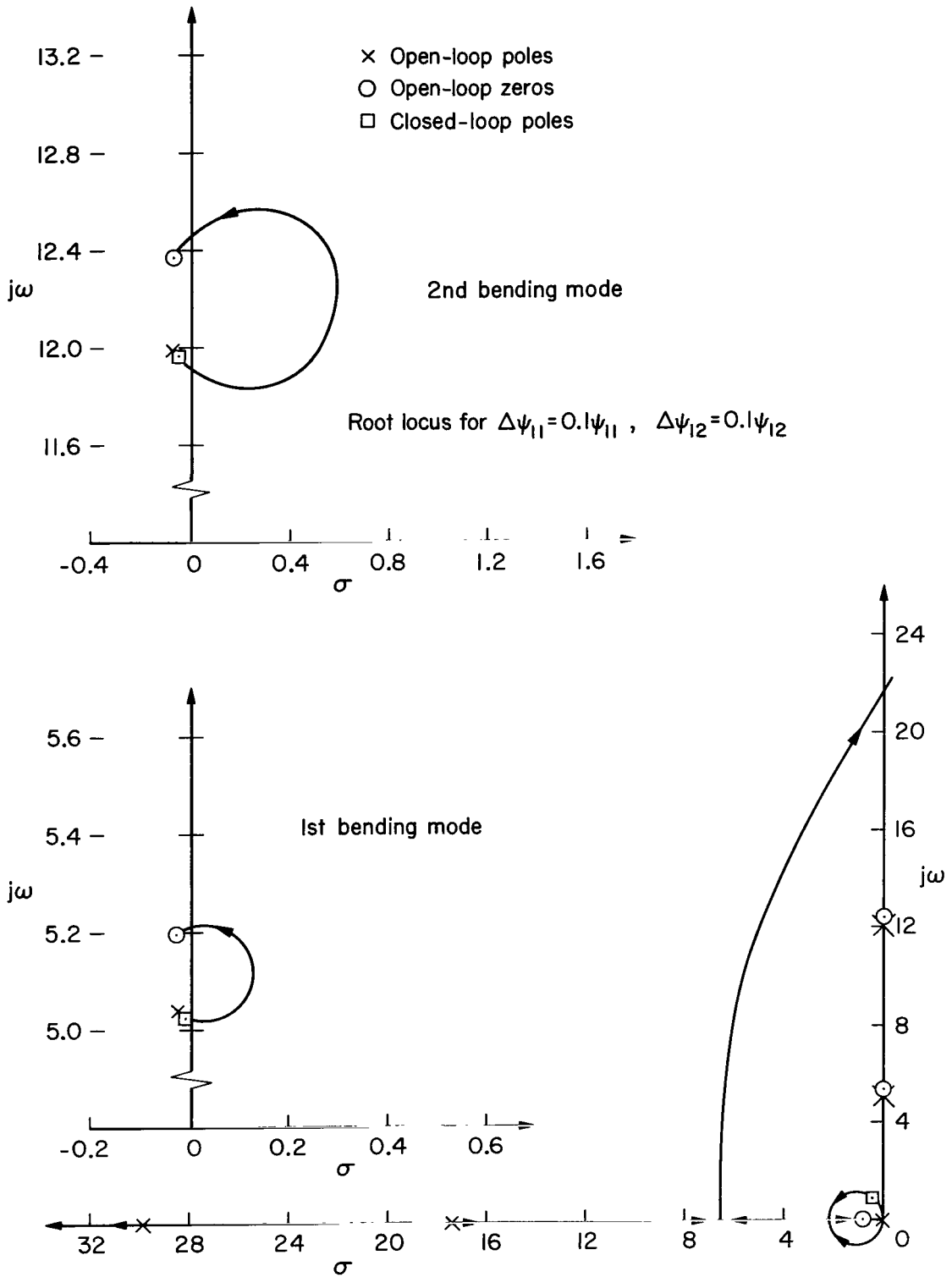

Figure 16.- Effect of modal errors on the root locus, both error coefficients negative, a_1 = -0.002043, a_2 = -0.002741.

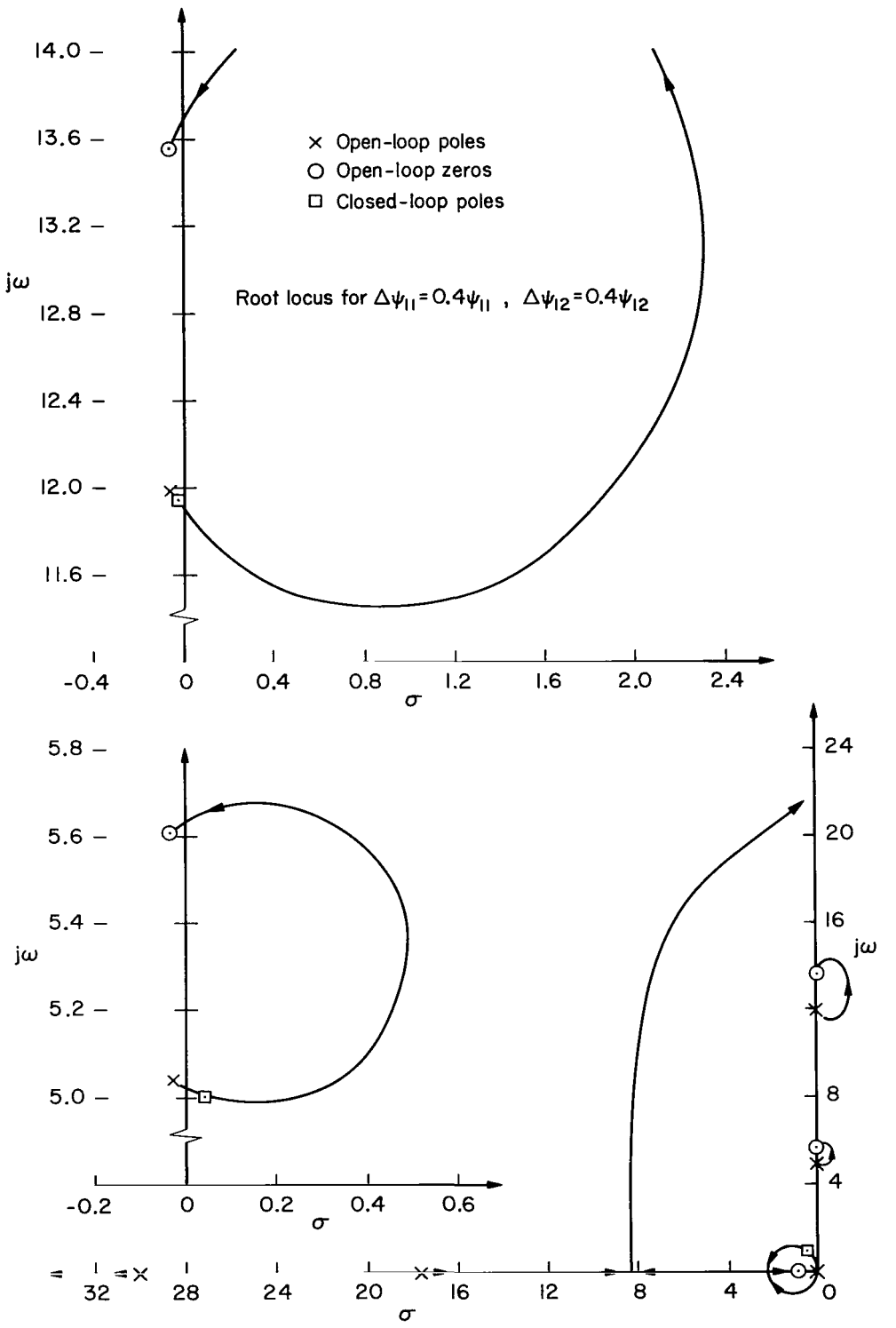

Figure 17.- Effect of modal errors on the root locus, both error coefficients negative, a_1 = -0.007011, a_2 = -0.009409.

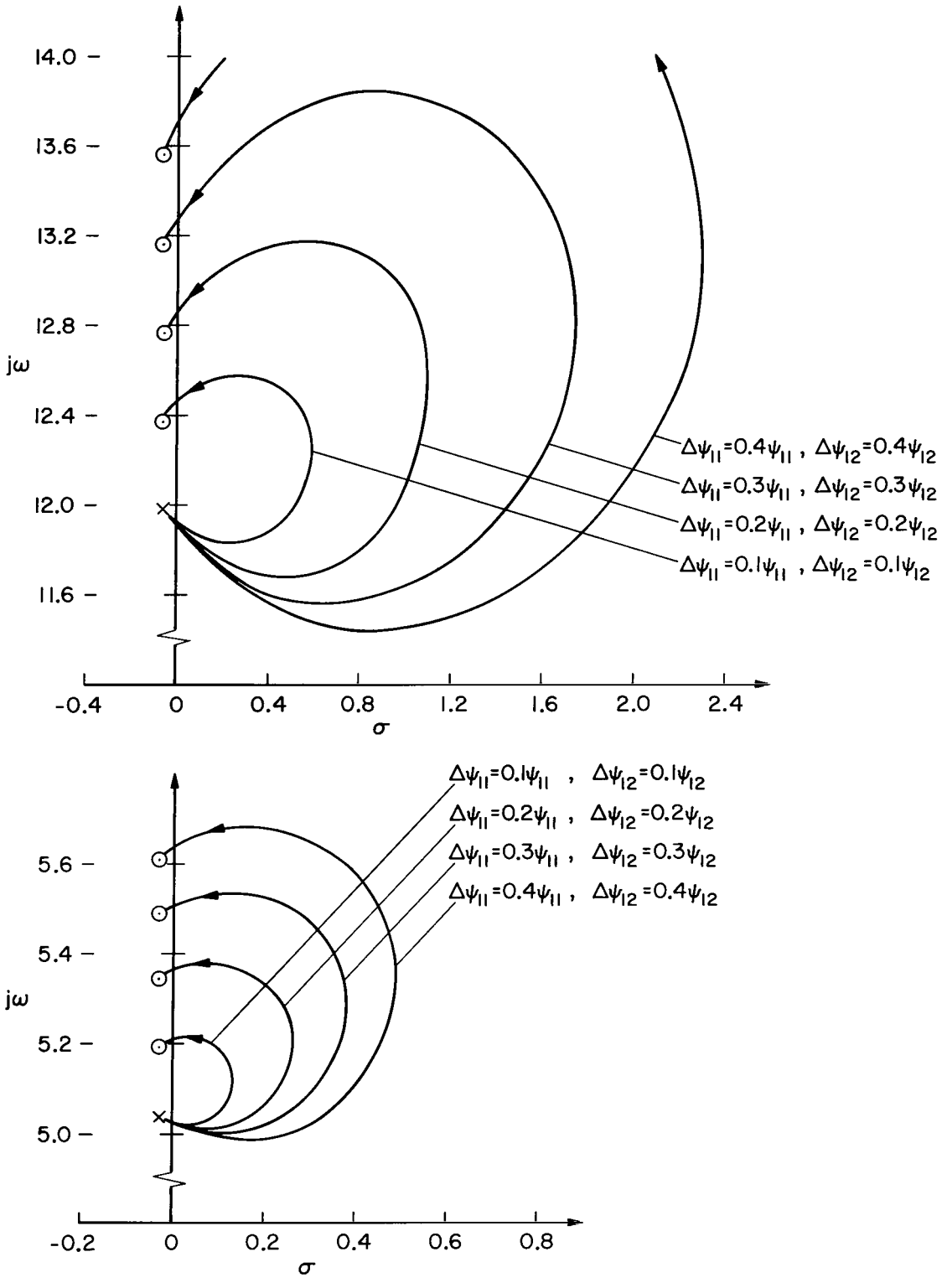

Figure 18.- Root-locus variations produced by positive error in mode 1 at sensor 1, and by positive error in mode 2 at sensor 1.

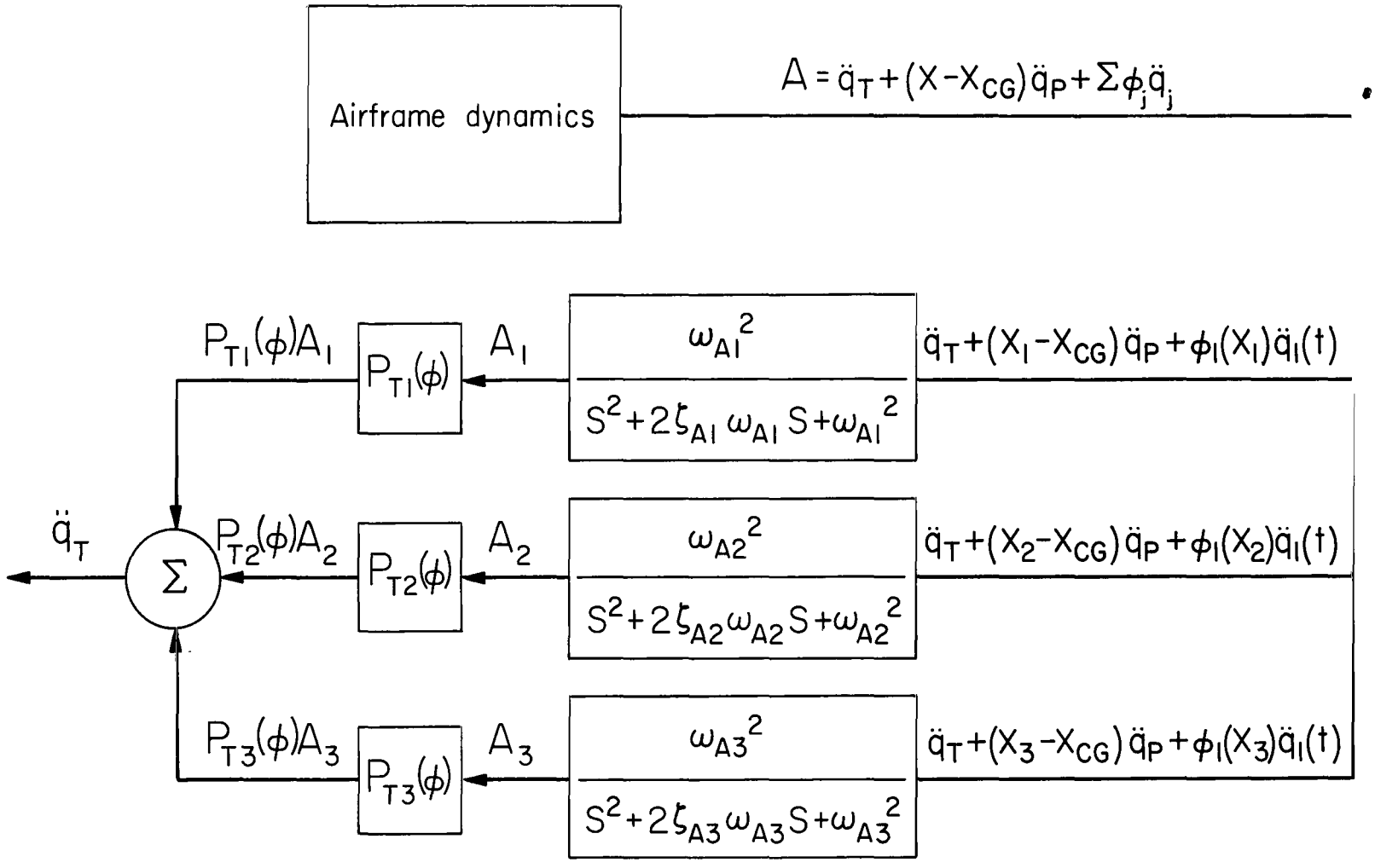

Figure 19.- Block diagram of system for processing accelerations in order to obtain the rigid-body translational acceleration.

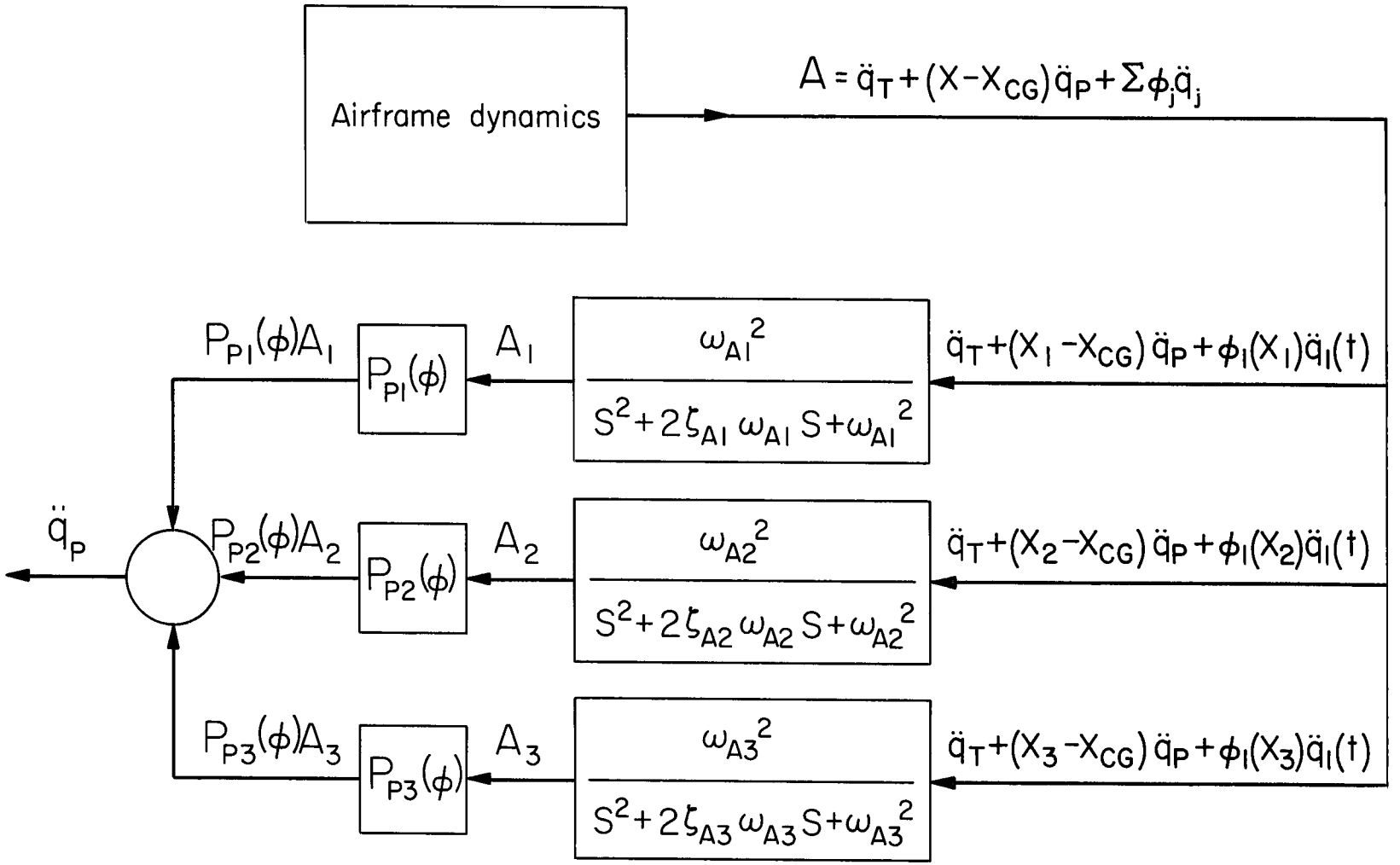

Figure 20.- Block diagram of system for processing accelerations in order to obtain the rigid-body pitching acceleration.

"The aeronautical and space activities of the United States shall be conducted so as to contribute . . . to the expansion of human knowledge of phenomena in the atmosphere and space. The Administration shall provide for the widest practicable and appropriate dissemination of information concerning its activities and the results thereof."

—NATIONAL AERONAUTICS AND SPACE ACT OF 1958

NASA SCIENTIFIC AND TECHNICAL PUBLICATIONS

TECHNICAL REPORTS: Scientific and technical information considered important, complete, and a lasting contribution to existing knowledge.

TECHNICAL NOTES: Information less broad in scope but nevertheless of importance as a contribution to existing knowledge.

TECHNICAL MEMORANDUMS: Information receiving limited distribution because of preliminary data, security classification, or other reasons.

CONTRACTOR REPORTS: Technical information generated in connection with a NASA contract or grant and released under NASA auspices.

TECHNICAL TRANSLATIONS: Information published in a foreign language considered to merit NASA distribution in English.

TECHNICAL REPRINTS: Information derived from NASA activities and initially published in the form of journal articles.

SPECIAL PUBLICATIONS: Information derived from or of value to NASA activities but not necessarily reporting the results of individual NASA-programmed scientific efforts. Publications include conference proceedings, monographs, data compilations, handbooks, sourcebooks, and special bibliographies.

Details on the availability of these publications may be obtained from:

SCIENTIFIC AND TECHNICAL INFORMATION DIVISION

NATIONAL AERONAUTICS AND SPACE ADMINISTRATION

Washington, D.C. 20546